DEEP RESISTIVITY MEASUREMENTS

IN THE FRASER VALLEY, BRITISH COLUMBIA

by

JOHN CRAIG SAMSON

B.Sc., University of British Columbia, 1967

A THESIS SUBMITTED IN PARTIAL FULFILMENT OF

THE REQUIREMENTS FOR THE DEGREE OF

MASTER OF SCIENCE

in the Department

of

GEOPHYSICS

We accept this thesis as conforming to the

required standard

THE UNIVERSITY OF BRITISH COLUMBIA

September, 1967

Department of GEOPHYSICS

The University of British Columbia
Vancouver 8, Canada

Date AUGUST 23, 1968

ABSTRACT

In the summer of 1967, dipole arrays were used to make deep resistivity soundings in the Fraser Valley of British Columbia. The large dipole moment of the input dipole (270 amp x 37 km) allowed input-to-measuring dipole spacings as great as 100 km.

Calculations show that Georgia Strait, which is spanned by the input dipole, should have little effect on layered earth potentials for the dipole to dipole spacings used in this survey.

A three-layer model with a resistive second layer (transverse resistance approximately 3000 times that of the upper layer) agrees well with the data. A more complicated four-layer model can be devised by using data from deep wells in the area. Interpretation of well and sounding data indicates that 500 m of conductive ocean and ocean sediments overlie 4-5 km of Tertiary and Cretaceous sedimentary rocks and 2 km of granitic rock. A conducting layer underlying the granitic rock may be the result of water saturation of the rocks at these depths.

TABLE OF CONTENTS

LIST OF TABLES

LIST OF FIGURES

APPENDIX

ACKNOWLEDGEMENTS

I would like to thank Dr. S. H. Ward for his many helpful suggestions and Dr. J. A. Jacobs for his encouragement and support during much of the project.

I am indebted to W. H. Cannon, R. D. Meldrum, P. Michalow, and T. Thorne for their time and effort spent in construction of equipment and in fieldwork. The contribution of equipment by the Pacific Naval Laboratories eased many experimental difficulties. The author is grateful to R. M. Shier and the British Columbia Hydro and Power Authority for their cooperation, without which this project would have been impossible.

I must also thank Drs. R. M. Ellis and G. K. C. Clarke for their critical reading of this thesis.

The arduous task of typing was accomplished by J. Kalmakoff and J. Copeland.

Throughout this research the author was supported by Pan American Petroleum Corp. and the National Research Council of Canada.

1 INTRODUCTION

1-1 Deep Resistivity Measurements in the Fraser Valley

In the summer of 1967, the British Columbia Hydro and Power Authority (B.C.H.P.A.) began testing a new direct-current ground return line running between the British Columbia mainland and Vancouver Island (Figure 1-1). The large input current (270 amp) and large input electrode separation (37 km) presented a unique opportunity for the measurement of deep resistivities in the Fraser Valley of British Columbia.

To take advantage of the B.C.H.P.A. tests, the University of British Columbia Department of Geophysics made potential measurements in various parts of the Fraser Valley and Delta. The position of the input system precluded the use of the more common Wenner and Schlumberger configurations. Consequently all measurements were made using dipole arrays.

In the past, numerous deep resistivity measurements in western North America have indicated that the lower crust varies from highly conductive to highly resistive (T. Cantwell et al [4], [5], H. S. Lahman et al [15], D. B. Jackson [11]). In addition, geomagnetic depth sounding data has implied that an anomalous conducting layer exists at twenty-five kilometers under much of the Cordillera region of western North America (B. Caner et al [3]). It was hoped that the measurements from the Fraser Valley area would help clarify other deep resistivity data and complement data obtained using geomagnetic depth sounding techniques.

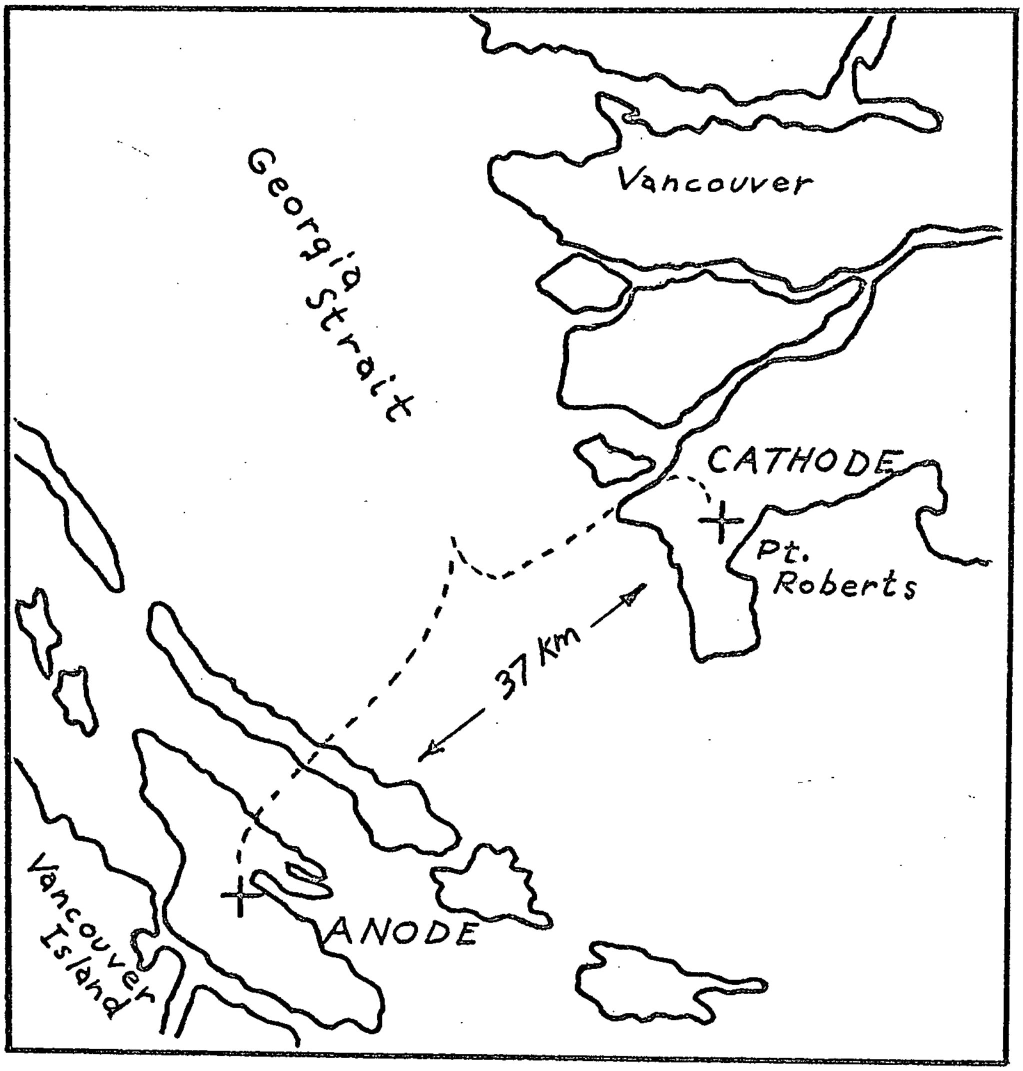

Figure 1-1 Location of input electrodes

1-2 Electrical Soundings

All direct-current resistivity surveys make use of the widely varying electrical resistivities of the materials of the earth. (Sea water has a resistivity of 0.5 ohm-m whereas quartz can have a resistivity as high as 10^{10} ohm-m.) Direct-current patterns are regulated to a large extent by geological features and their inherent resistivity contrasts, and thus present a proficient method for determining subsurface features.

In general the apparatus used is very simple, consisting of

(a) input electrodes and current supply

(b) two electrodes and a voltmeter to measure potentials at various points.

Direct-current resistivity *soundings* use electrodes placed in the earth near the surface to determine resistivities at various depths. Soundings are taken by varying the separation of the input electrodes or by varying the separation between input and measuring electrodes. Figure 1-2 shows the various dipole configurations in use. The dipole array is further defined as ideal ($a,b \ll r_1,r_2,r_3,r_4$) or non-ideal (one or both of a and b are large). In this thesis the separation between the dipoles of an ideal dipole array will be denoted by r_2, otherwise parameters are as defined in Figure 1-2(a).

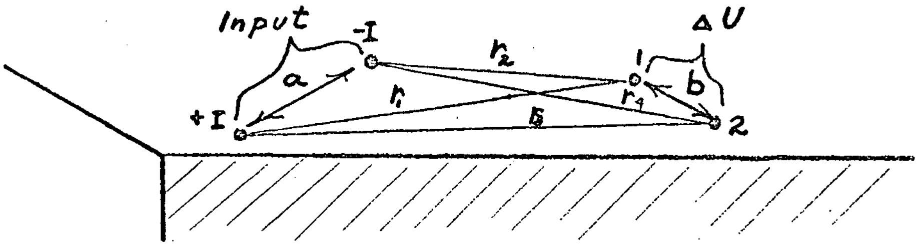

(a) General dipole array - Input dipole remains fixed. Soundings are taken by moving measuring dipole.

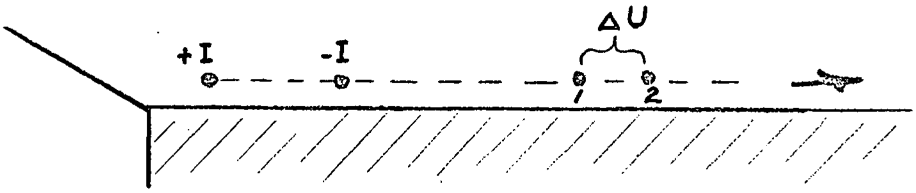

(b) Polar dipole - Measuring dipole is moved in line with input dipole.

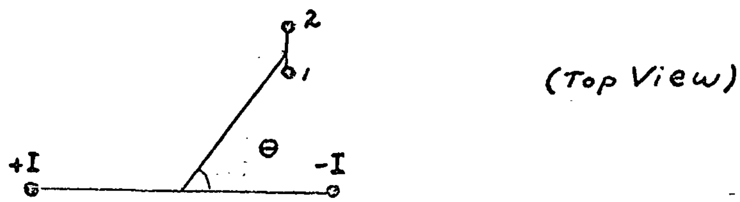

(c) Perpendicular dipole - Measuring dipole always remains oriented perpendicular to the line of the input dipole.

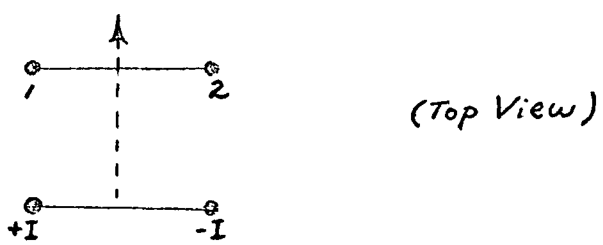

(d) Equatorial dipole - Measuring array moves outward along centre line of input dipole.

Figure 1-2 Common dipole configurations

1-3 Apparent Resistivity

In order to facilitate interpretation of direct-current potential measurements, the concept of *apparent resistivity* is often used. If the earth were a homogeneous, isotropic, half-space, one would find

$$\rho = f\ (\Delta U,\ I,\ k) \qquad (1\text{-}1)$$

where k is some variable depending on the configuration of the electrodes; I is input current; ΔU is potential difference at the measuring dipoles. In this case f is defined such that the resistivity ρ remains constant for varying k (as is expected for a homogeneous earth).

For an inhomogeneous earth, the same function f is used to define an apparent resistivity. In this case ρ varies as k is varied.

To determine f assume once again that the earth is a homogeneous, isotropic half-space with resistivity ρ, in contact with an insulating half-space, air. Using Ohm's law and conservation of charge, one finds $\nabla^2 U = 0$ everywhere except at a current source or sink. For the configuration of Figure 1-3 the solution in cylindrical coordinates is

$$U\ (r,\ z) = \frac{I\rho}{2\pi\ (r^2 + z^2)^{\frac{1}{2}}} \qquad (1\text{-}2)$$

(G. Keller and F. Frischknecht [12])

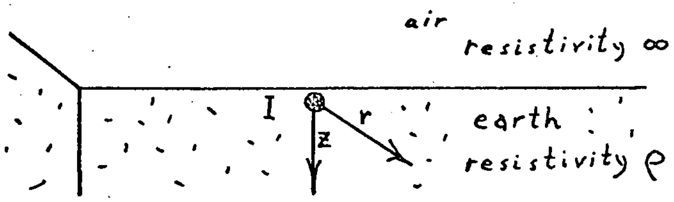

Figure 1-3 Point source in an homogeneous earth

Using the superposition principle, the potential for two input electrodes +I and -I (Figure 1-2(a)) is

$$U(1) = \frac{I\rho}{2\pi r_1} - \frac{I\rho}{2\pi r_2} \tag{1-3}$$

and

$$\Delta U = U(1) - U(2) = \frac{\rho I}{2\pi}\left[\frac{1}{r_1} - \frac{1}{r_2} - \frac{1}{r_3} + \frac{1}{r_4}\right] \tag{1-4}$$

Consequently

$$\rho = \frac{2\pi\Delta U}{I}\left[\frac{1}{r_1} - \frac{1}{r_2} - \frac{1}{r_3} + \frac{1}{r_4}\right]^{-1} \tag{1-5}$$

Where the earth is inhomogeneous an *apparent resistivity*, denoted ρ_a , is calculated using equation 1-5.

Consider for example an ideal polar dipole over a two-layer earth. The apparent resistivities calculated using Equation 1-5 would be as given in Figure 1-4. At small r_2 , the apparent resistivity is equal to the resistivity of the upper layer; at large r_2 the apparent resistivity is equal to the resistivity of the lower layer (this is intuitively expected).

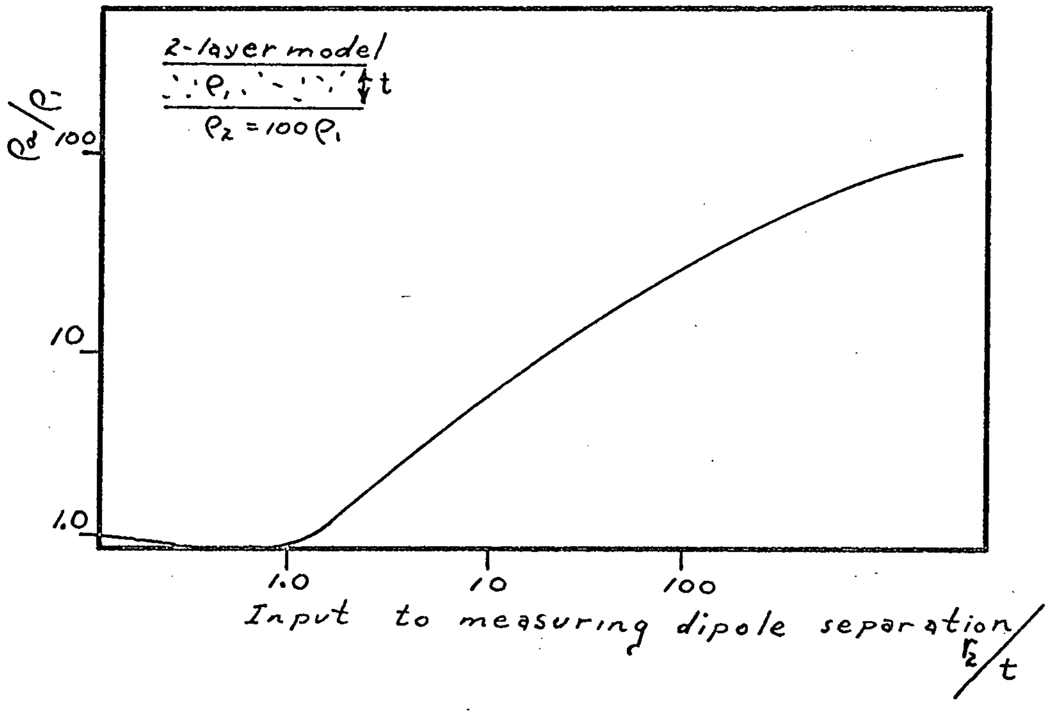

Figure 1-4 Apparent resistivity for an ideal polar dipole over a two layer earth

1-4 Characteristics of Electrical Soundings

1-4-1 Effective Sounding Depth

Of primary concern is the depth at which direct-current resistivity soundings can detect resistive discontinuities. In general this depth depends on the particular electrode configuration as well as the subsurface geology.

A criterion for measuring effective sounding depths can be found by considering the apparent resistivity curves for a two-layer earth, with top layer of resistivity ρ_1, thickness t, and bottom layer of infinite resistivity (Figure 1-5).

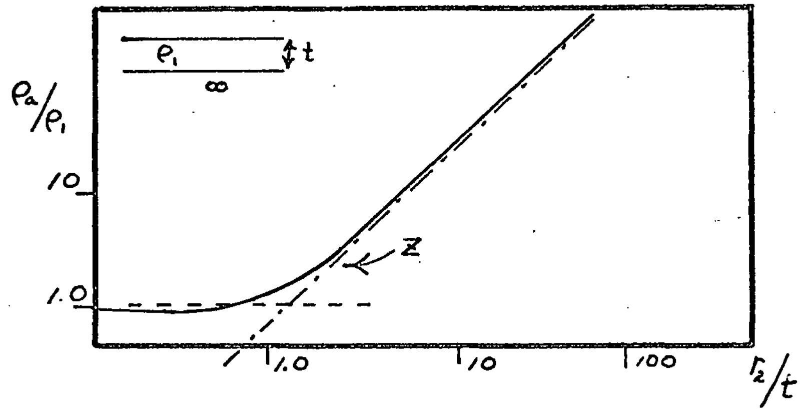

Figure 1-5 Apparent resistivity for an ideal polar dipole over a two-layer earth with insulating basement.

One can see from the graph that the rounding of the resistivity curve, indicating the presence of the second layer, is evident when line Z, tangent to the resistivity curve for large r_2, intercepts $\rho_a/\rho_1 = 1$ or $\rho_a = \rho_1$. The equation for Z can be found in the following manner:

At large distances from a current source, the current density j has a cylindrical symmetry. Thus the electric field is given by

$$E = \rho_1 j = \frac{I\rho_1}{2\pi rt} \tag{1-6}$$

where r is the distance from the source I . For inputs $+I$ and $-I$

$$E \simeq \frac{I\rho_1}{2\pi t}\left[\frac{1}{r_1} - \frac{1}{r_2}\right] \tag{1-7}$$

where r_1 is the distance from $+I$

r_2 is the distance from $-I$

This gives the potential for a polar dipole array at large input to measuring dipole separations

$$\Delta U = E\Delta r = \frac{I\rho_1 b}{2\pi t}\left[\frac{1}{r_1} - \frac{1}{r_2}\right] \tag{1-8}$$

where b is the measuring electrode separation. Using Equation 1-5 gives for line Z

$$\rho_a = \frac{\rho_1}{t}\left[\frac{1}{r_1} - \frac{1}{r_2}\right]\left[\frac{1}{r_1^2} - \frac{1}{r_2^2}\right]^{-1} \tag{1-9}$$

The point where this line intercepts $\rho_a = \rho_1$ is given by

$$t = \left[\frac{1}{r_1} - \frac{1}{r_2}\right]\left[\frac{1}{r_1^2} - \frac{1}{r_2^2}\right]^{-1} \tag{1-10}$$

Figure 1-6 gives the depth t at which a boundary can be detected using a polar dipole configuration.

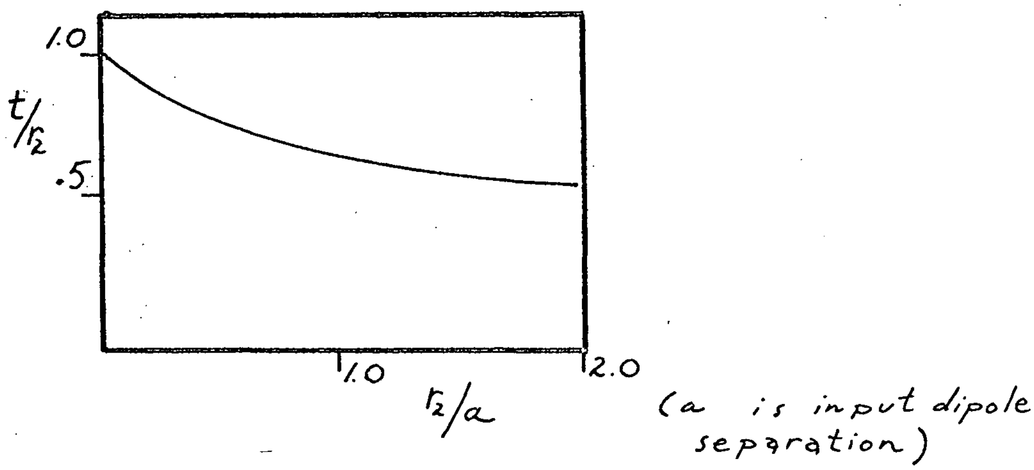

Figure 1-6 Effective sounding depth of a polar dipole array over a two-layer earth

The effective sounding depths for dipoles over multilayered earths are much less than those for two-layer earths. Figure 1-7 gives apparent resistivity curves for an ideal polar dipole array over a three-layer earth. Evidently the second boundary, indicated by a dip in the resistivity curve, is noticeable only when $r_2 \approx 20(t_1 + t_2)$. To detect a discontinuity 5 km deep would require an array spacing of 100 km.

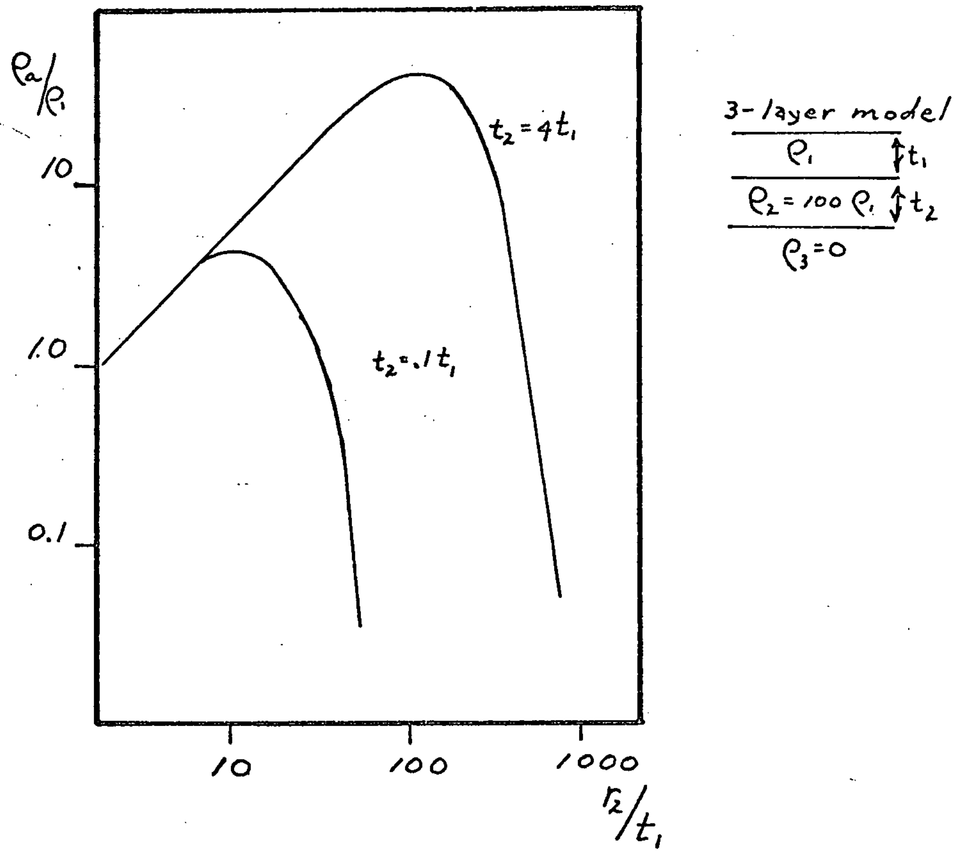

Figure 1-7 Apparent resistivity for an ideal polar dipole over a three - layer earth.

1-4-2 Maximum Electrode Spacings

Sounding depths are also limited by the maximum separation between input and measuring dipoles. In most cases this separation is limited, not by equipment sensitivity, but by natural and industrial telluric noise. M. N. Berdichevskii [1] has indicated that

$$E_T = D\rho^{\frac{1}{2}}$$

where E_T is the natural telluric field and D is a constant. From data collected in the Fraser Valley survey, it is estimated that

$$E_T \approx 3\cdot(10^{-5})\rho^{\frac{1}{2}} \tag{1-11}$$

ρ in ohm-m

(at 0.02 Hz)

Using Equation 1-4 which defines the potential for a dipole configuration on a homogeneous earth gives, for a polar dipole

$$\Delta U = \frac{-\rho I}{2\pi} \; b\left[\frac{1}{r_2 r_4} + \frac{1}{r_1 r_3}\right]$$

$$\approx \frac{-\rho I b}{2\pi}\left[\frac{1}{r_2^{\,2}} + \frac{1}{(r_2 + a)^2}\right] \tag{1-12}$$

(for small b)

Assuming that a signal can be detected when the signal-to-noise ratio is 0.1 (see Appendix A-2), the maximum separation will be given by

$$\frac{\rho I b}{2\pi}\left[\frac{1}{{r_2}^2} + \frac{1}{(r_2 + a)^2}\right] = 10^{-5}\rho^{\frac{1}{2}}b \qquad (1\text{-}13)$$

For small a

$$r_2 = (1.8)(10^3)\rho^{\frac{1}{4}}I^{\frac{1}{2}} \qquad (1\text{-}14)$$

Equation 1-14 indicates that the effective resistivity of an area will have a negligible influence on maximum spacings, provided input and measuring dipoles are in areas of equivalent subsurface geology. With ρ = 100 ohm-m and I = 250 amp , r_2 is 100 km. This corresponds to an effective sounding depth of 50 km (Figure 1-6).

1-4-3 Ambiguities in Interpretation

Topographical changes and near-surface resistivity anomalies often cause a large scatter in the data from sounding surveys. In many cases this scatter is so great that it is impossible to use resistivity data alone to distinguish between two completely different models.

Topographical effects are very difficult to determine. For a conductive overburden over a resistive basement, a common situation, topographical effects can be approximated analytically, provided elevation changes are very broad features when compared to first-layer thickness. ($d >> t$. See Figure 1-8.)

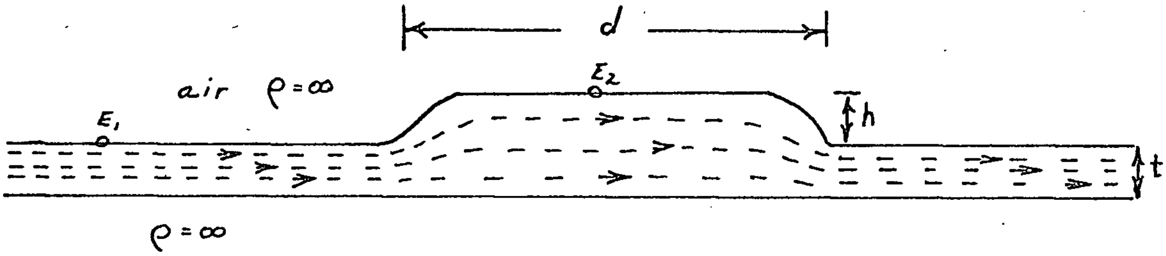

Figure 1-8 Current density in a two-layer earth

If the source is sufficiently far away that current density j can be considered continuous, one would expect

$$j \propto t^{-1} \quad \text{and} \quad E \propto t^{-1}$$

Consequently

$$\frac{E_2}{E_1} = \frac{t}{t + h} \tag{1-15}$$

Even if h were $1/2t$, E_2 would still be $2/3E_1$. For sharper topographical changes, however, the effect would be much more severe.

Possibly one of the greatest sources of concern in dipole soundings is the array's extreme sensitivity to near-surface lateral variations in resistivity. An example illustrates the problem very clearly. In Figure 1-9 the body having resistivity ρ_2 represents a near-surface anomaly.

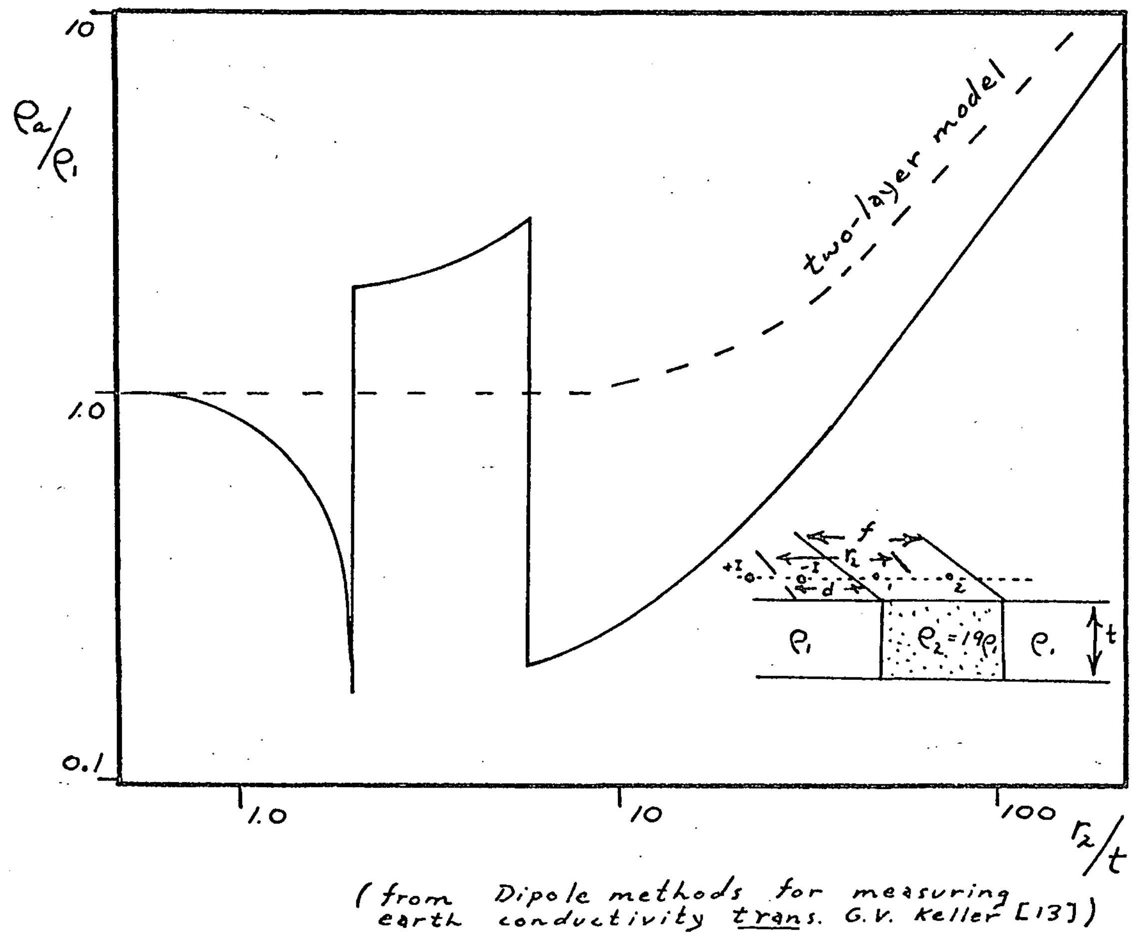

Figure 1-9 Apparent resistivity for an ideal polar dipole expanded perpendicular to the contact of a resistive anomaly.

There is clearly a significant variation in apparent resistivity. A number of such anomalies near the surface would cause resistivity values to vary, apparently at random, by factors of three or more, giving a wide scatter of data points in an area that has a very simple overall geology. In such cases, the range of models which fit the data becomes very large, and good geological control is needed if one is to choose a reasonable model. It is therefore imperative that the dipoles be located in an area which has a very homogeneous upper layer.

An example of the similarity in apparent resistivity curves for two very different models is given in Figure 1-10.

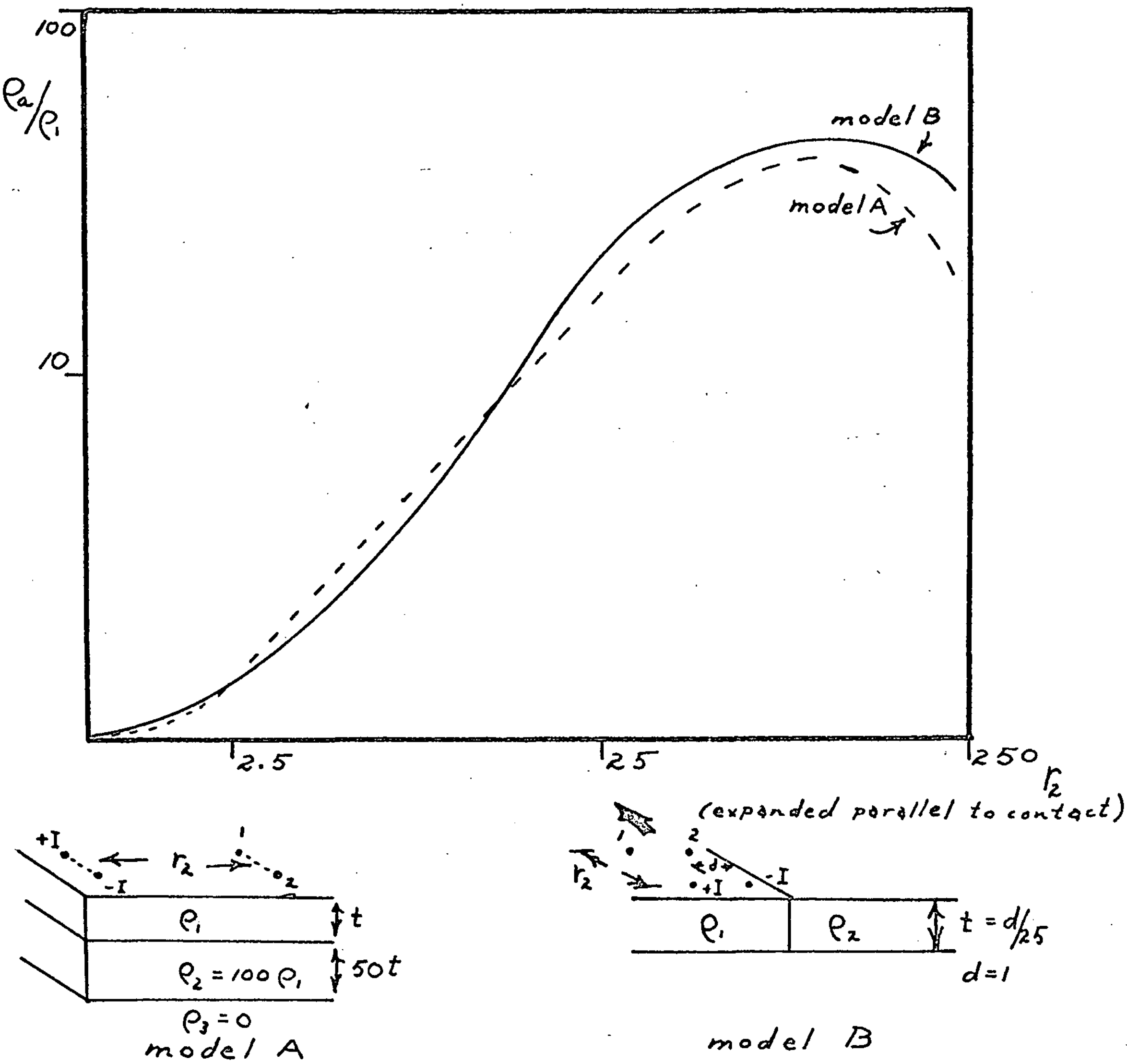

Figure 1-10 Apparent resistivity for equatorial dipoles over two different earth models.

Obviously it would be quite difficult to determine from one sounding, the geological conditions that prevail, especially if the sounding data is scattered over values that vary by a factor of two or three. Some of the ambiguity may be eliminated by using two different types of arrays to obtain two different sounding curves for a given area.

2 DESCRIPTION OF THE SURVEY

2-1 Geology of the Fraser Valley and Delta

The following information was obtained from articles by J. A. Roddick [21], P. Misch [17], R. I. Walcott [25], and W. S. Hopkins [9].

The Fraser Valley, which lies in the western part of the Cordilleran volcanic and orogenic belts, is a structural basin which began to subside during middle Eocene. At present, ninety percent of the area is below 30 m. The valley proper is covered by a superficial layer of Quaternary alluvium overlying Tertiary and Cretaceous sedimentary rocks. In the vicinity of Vancouver, the Tertiary rocks (conglomerates, shales, sandstones) have a probable depth of 700 m with a dip of 15° to the south. Near Point Roberts, on the United States - Canada border, 300 m of Quaternary sediments overlie 2700 m of terrestrial and marine Tertiary rocks and at least 1000 m of upper Cretaceous sedimentary rocks. Further up the valley, near Pitt Meadows, well data indicates Quaternary deposits are at least 300 m thick. Outcrops of terrestrial Tertiary rocks (conglomerate, sandstone) are evident near Canadian Sumas Mountain but very little information on their thickness has been obtained.

To the north of the valley are the granitic rocks of the Coast Mountains, ranging in elevation from 1000 - 1500 m. This is a complex intrusion, probably mid-Jurassic to Tertiary age, of metamorphic rocks consisting for the most part of quartz diorite with smaller amounts of granodiorite and gabbro.

The southern part of the valley is flanked by the 1000 m high foothills of the Cascade Mountains. The basement here is metaquartz diorite and orthogneiss of Middle Devonian age (P. Misch [17]). Above this, separated by a nonconformity, is a thick sequence of Paleozoic volcanic (basalt and andesite) and sedimentary rocks. During the late Cretaceous to early Tertiary, deposition in a continental trough produced sandstone and conglomerates.

For the purposes of resistivity measurements, the rocks may be included in three distinct groups. These are:

<u>Low Resistivity</u>

0.5-5 ohm-m	ocean and new ocean sediments

<u>Intermediate Resistivity</u>

10-30 ohm-m	Quaternary alluvium
10-50 ohm-m	Tertiary marine sedimentary rocks
15-400 ohm-m	Tertiary terrestrial sedimentary rocks
15-400 ohm-m	Cretaceous sedimentary rocks
130-500 ohm-m	Miocene and Pliocene volcanics

<u>High Resistivity</u>

500-2000 ohm-m	Mesozoic intrusives (quartz diorite gabbro)

Surface geology is shown in Figure 2-1. (Resistivities for the sedimentary rocks are from well data for three wells in the area, Richfield Pure Pt. Roberts, Richfield Pure Abbotsford, and Richfield Pure Sunnyside. Other values are from G. V. Keller and F. C. Frischknecht [12].)

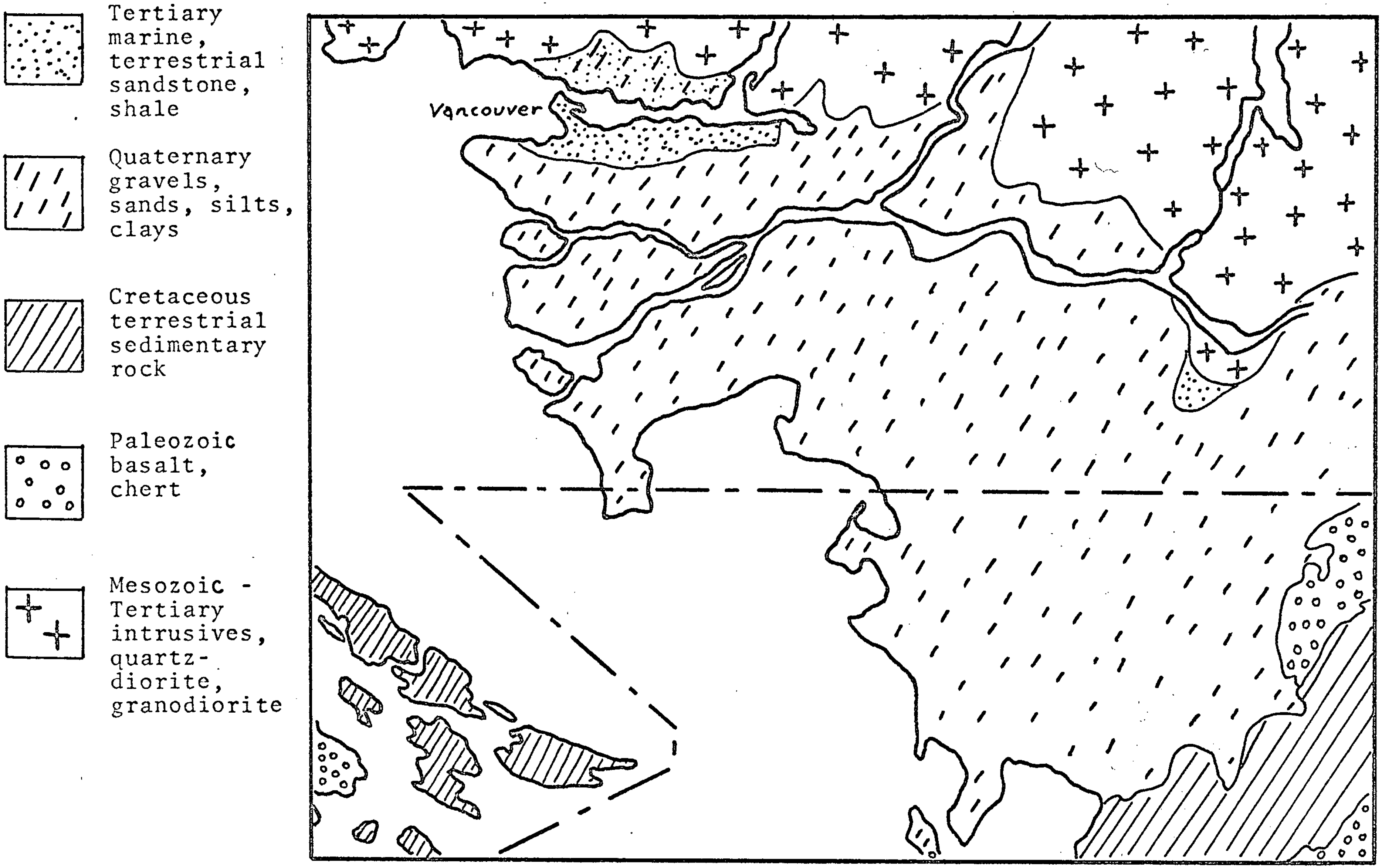

Figure 2-1 Surface geology of the Fraser Valley and Delta.

2-2 Equipment

The input circuit was part of a new B.C.H.P.A. direct-current ground return line. The total resistance of the whole circuit, including electrodes, was 4 ohm. Input current was cycled with a three minutes ON two minutes OFF repetition. Total variation of input current was never greater than 2% (263-269 amp). Most variation of input current was caused by a gradual heating of the input circuit over the period of operation. The positions of the input electrodes are given in Figure 2-3. The input monitor is given in Appendix A-1.

A block diagram of the equipment used for the potential measurements in this survey is given in Figure 2-2. Circuit diagrams and special characteristics of the equipment are given in Appendix A-1. The electrodes (1) were copper-copper sulfate solution, housed in porous porcelain containers. All electrical connections were copper to copper. Low-tension, plastic-coated copper wire (2) was used for all grounded circuits. Stray direct-current potentials were balanced with an external bias system (3). In order to prevent 60 Hz overload of the amplifier (5), a 60 Hz rejection filter (4) was used. All subsequent connections used two-strand coaxial cable with external shields grounded to the cabinets of the instruments. Amplifier (5) was a low frequency "chopper" amplifier. The input impedance of this system was about one megohm.

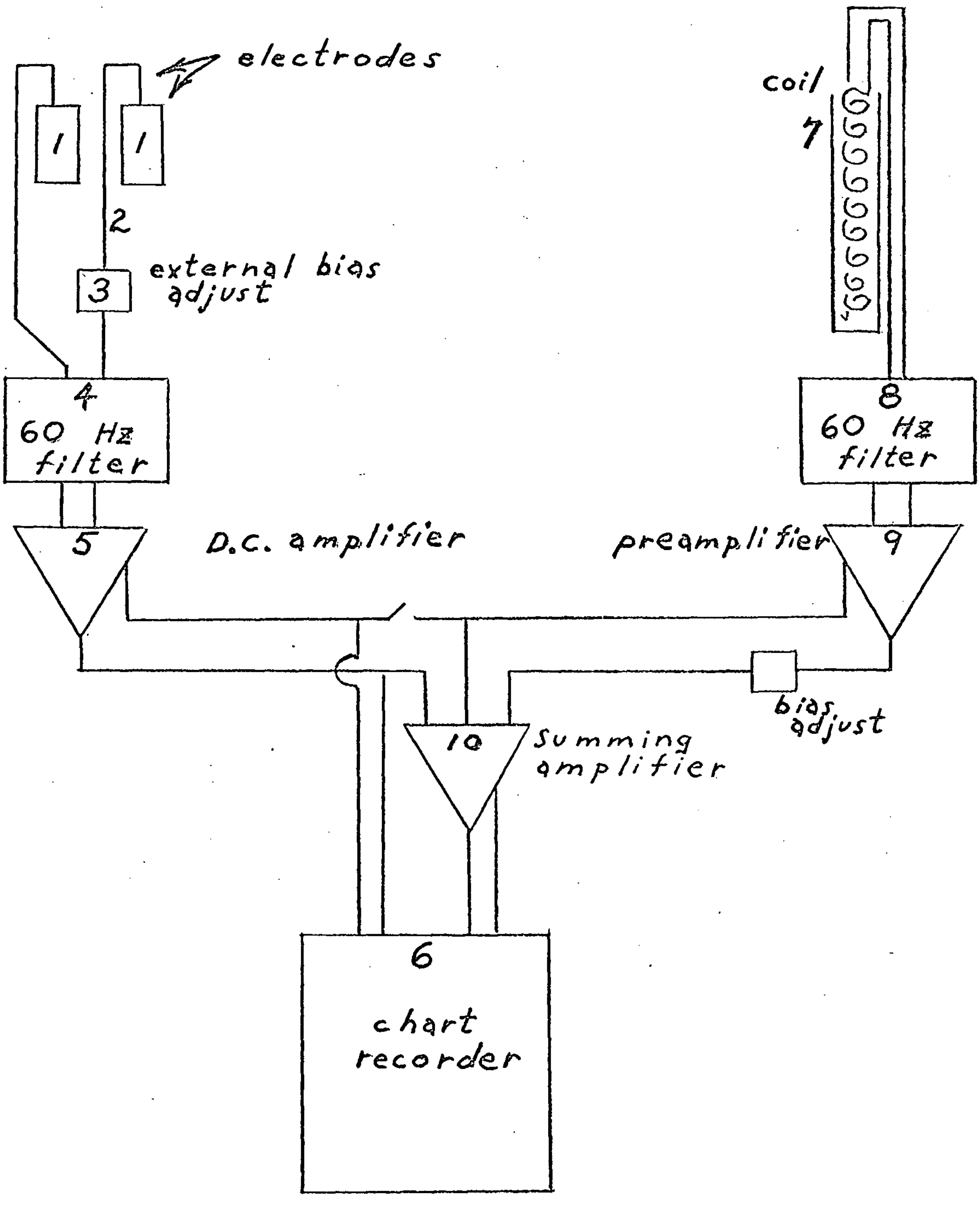

Figure 2-2 Potential measuring apparatus

A channel to monitor the earth's magnetic field was included in an effort to deal with the telluric noise problem. (All potential measurements were made during the day. Consequently noise values were generally high.) The iron-core coil (7) and "chopper" amplifier (9), were similar to those used at the University of British Columbia's magnetic station on Westham Island. Filter (8) was the same as that used on the ground line. The summing amplifier (10) was designed as a low-pass filter. Provision was made to subtract the telluric and magnetic signals if relative phase shifts were not too great.

2-3 Procedure

All potential measurements were made on the alluvial deposits of the Fraser Valley in order to take advantage of

a) good elevation control

b) ease in determining locations (There are many roads in this area.)

c) homogeniety of the superficial alluvial sediments

d) reduced values of telluric noise (when distant from cities)

Initial measurements, to check the operation of the equipment and to determine the thickness and resistivity of the Quaternary sediments, were taken along a line running northwest from the input cathode (line #1 in Figure 2-3). All measuring-electrode spreads were aimed at the cathode of the input system. A second series of measurements was made following an east-west line along the valley (line #2). At each location, two orientations of the measuring electrode were used in an attempt to reduce any ambiguities which might result from lateral variations in resistivity. Orientations were east-west and north-south, following the direction of the roads in the area. Telluric noise limited cathode-to-measuring-electrode separations to 76 km. A few measurements to the northeast of the cathode were obtained, but the B.C.H.P.A. terminated operation of the input system before a large number of measurements could be made.

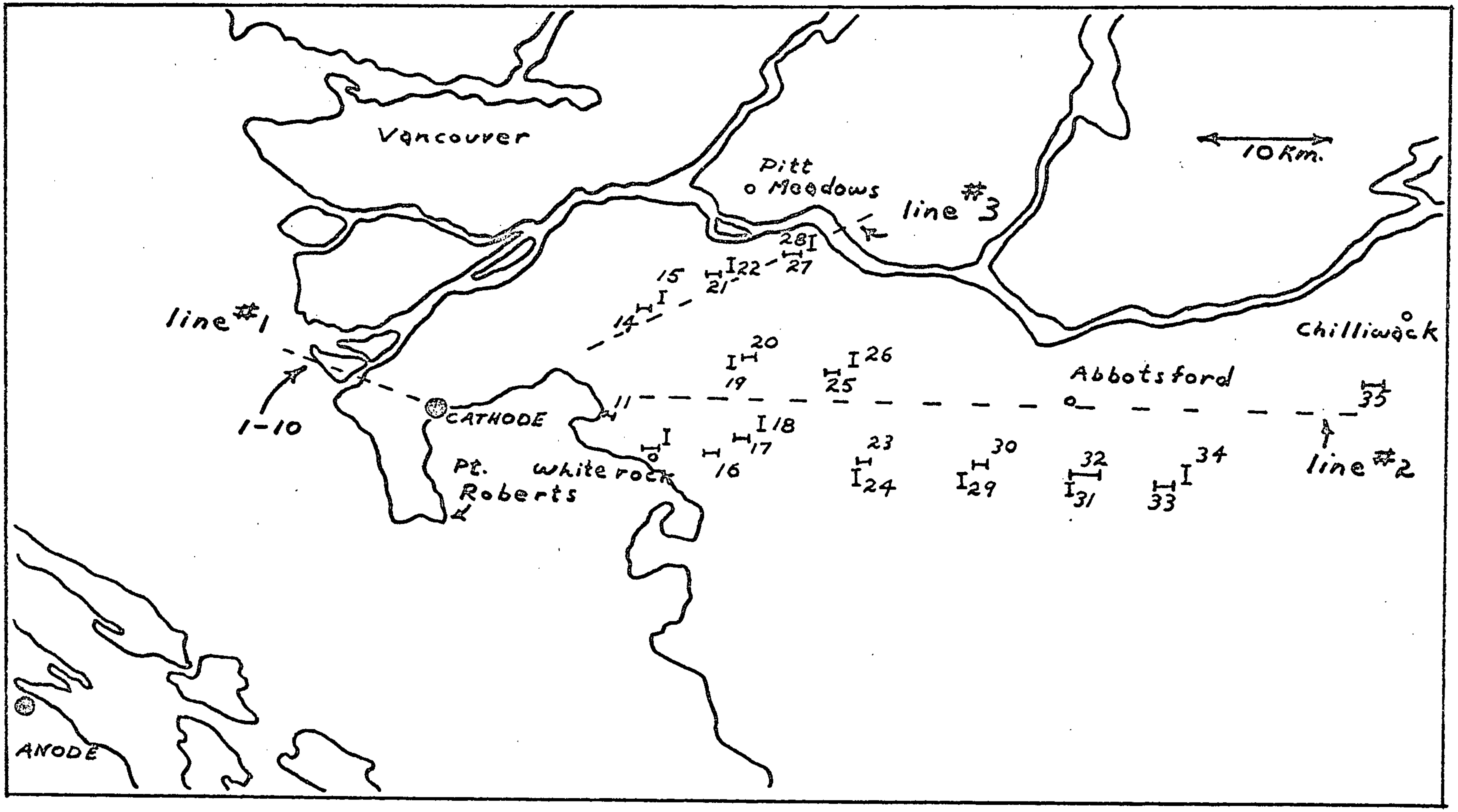

Figure 2-3 Measuring dipole locations.

At each location the electrodes were buried one-third to one-half meter below any existent organic layer. To reduce contact resistance, varying amounts of copper sulfate solution, depending on the moisture content of the ground, were poured around the electrodes. Electrode separations were determined by marks on the connecting cables or by measuring the distance with a large tape measure. (Errors may be as large as 5% because of changes in terrain along roads and coiling of the cable.) Before recording the signal, the resistance of the ground line was measured to determine if there were any poor contacts in the line and to determine the approximate contact resistance of the electrodes. The signal was then recorded at a chart speed of 0.5 mm/sec.

When the signal-to-noise ratio was large (1.0 or better), only the telluric system was used and only enough cycles were recorded to permit a good visual estimate of the signal amplitude. (A definition of *signal-to-noise ratio* is given in Appendix A-2.) At stations where the noise level was significant, both magnetic and telluric channels were used. Recording time was regulated by the estimated amount of noise present. On occasion as many as 20 cycles were recorded.

2-4 Data Analysis

Signal amplitudes were estimated visually from records if signal-to-noise ratios were greater than 1.0. With moderate noise (signal-to-noise 0.2), the signal was detected by visually comparing the magnetic and telluric channels. When the signal turned on or off a "spike" appeared on the magnetic channel, otherwise, except for phase shifts, the two records appeared the same (Figure 2-4).

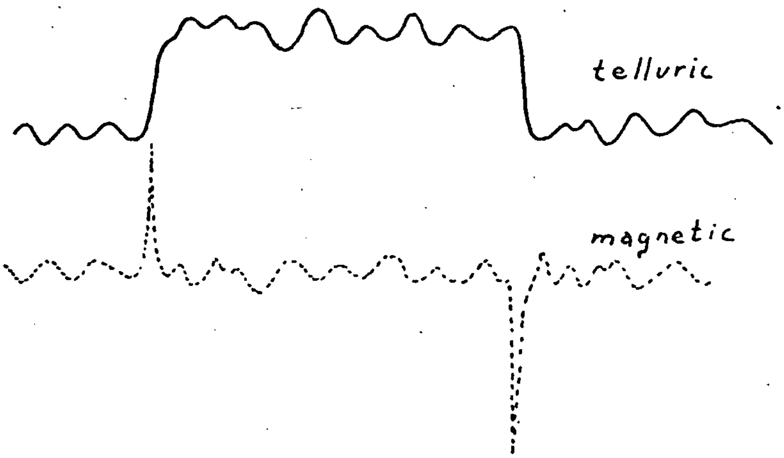

Figure 2-4 Comparison of recordings on magnetic and telluric channels.

In some cases signal-to-noise ratios could be improved by phase shifting and subtracting the magnetic record from the telluric record. (At times this improved signal-to-noise ratios by a factor of 10.)

At very large noise levels, the above methods did not prove at all effective. It was necessary, under these circumstances, to estimate signal amplitudes from the amplitude of the first four harmonics of the input signal. (See Appendix A-2.) Errors from visual estimates were probably no greater than 10% and from using the harmonics no greater than 20%.

Apparent resistivities were calculated using Equation 1-5 and plotted on log-log graphs with parameters ρ_a , apparent resistivity, and r_2 , distance between measuring dipole and cathode.

Estimates of the error in the calculations were made using the maximum values for instrument (see Appendix A-1) and reading error.

No terrain corrections were applied to the data. Corrections for the effects of a near-surface resistive anomaly near Abbotsford will be considered later.

3 DATA AND INTERPRETATION

3-1 Data

Table 3-1 gives a summary of the data for each location. The apparent resistivity values are plotted in Figure 3-1.

It is evident from the graph and from the table that values at positions 29, 31, and 32 are anomalously high. All these measurements were taken in the vicinity of Abbotsford where there is reason to believe that the basement rock is especially close to the surface. R. I. Walcott [25] conjectures that a small gravity high in the area may be caused by a thick sequence of gabbroic rocks, marginal to the Coast Mountains, underlying the Tertiary sediments and Pleistocene deposits. Values corrected to eliminate the effect of this resistive body would be a factor of two or three less than the measured apparent resistivities. (The effects of resistive bodies on dipole soundings are given in Figure 1-9.) The corrections are indicated by arrows on the graph.

TABLE 3-1 SUMMARY OF DATA

POSITION	LINE #	r_2 (km)	b (m)	ELECTRODE RES. (ohm)	ELEV. (m)	ORIENT.	POTENTIAL (mv)	RESISTIVITY (ohm-m)	EST. ERROR
1	1	.321	85.7		<3		55.6	1.5	<10%
2	1	.88	76.5		<3		13.9	2.9	<10%
3	1	.95	89.9		<3		11.5	2.9	<10%
4	1	1.48	137.		<3		12.	4.9	<10%
5	1	2.51	224.	65	<3		11.	7.8	<10%
6	1	3.61	155.	200	<3		5.8	11.9	<10%
7	1	4.67	325.	-	<3		6.7	12.2	<10%
8	1	6.34	175.	-	<3		4.1	22.	<10%
9	1	7.90	299.	-	<3		4.3	23.	<10%
10	1	11.3	259.	-	<3		3.2	41.	10%
11	2	11.1	305.	220	<3	E-W	4.2	47.	<10%
12	2	19.0	305.	225	30	E-W	1.6	52.	10%
13	2	19.5	305.	900	30	N-S	0.85	103.	<10%
14	3	19.5	305.	1,660	50	E-W	0.95	39.	15%

TABLE 3-1 (cont.)

POSITION	LINE #	r_2 (km)	b (m)	ELECTRODE RES. (ohm)	ELEV. (m)	ORIENT.	POTENTIAL (mv)	RESISTIVITY (ohm-m)	EST. ERROR
15	3	19.4	305.	1,300	50	N-S	0.30	17.	10%
16			UNBALANCED ELECTRODES - NO PROPER RECORDINGS						
17	2	23.8	305.	-	30	E-W	0.83	43.	<10%
18	2	24.0	305.	1,800	30	N-S	0.27	120.	10%
19	2	23.1	305.	50	13	N-S	0.50	112.	20%
20	2	23.1	305.	130	13	E-W	0.82	41.	10%
21	3	24.6	305.	200	10	E-W	0.46	29.	10%
22	3	24.7	305.	-	10	N-S	0.013	1.5	15%
23	2	29.8	610.	24,000	70	E-W	2.0	91.	10%
24	2	29.8	305.	110	70	N-S	0.83	110.	10%
25	2	30.5	303.	75	10	E-W	0.40	37.	15%
26	2	30.5	305.	152	10	N-S	0.25	138.	15%
27	3	33.9	684.	522	15	E-W	0.51	29.	20%
28	3	34.4	684.	240	15	N-S	0.32	42.	10%
29	2	39.0	305.	480	50	N-S	0.48	280.	10%

TABLE 3-1 (cont.)

POSITION	LINE #	r_2 (km)	b (m)	ELECTRODE RES. (ohm)	ELEV. (m)	ORIENT.	POTENTIAL (mv)	RESISTIVITY (ohm-m)	EST. ERROR
30	2	39.6	564.	380	50	E-W	.30	32.	15%
31	2	48.4	305.	18,000	80	N-S	.60	650.	10%
32	2	47.7	1525.	4,600	80	E-W	4.5	250.	20%
33	2	58.7	684.	215	<15	E-W	.23	39.	15%
34	2	58.7	690.	250	<15	N-S	.11	87.	20%
35	2	76.1	684.	165	<15	E-W	.10	40.	20%

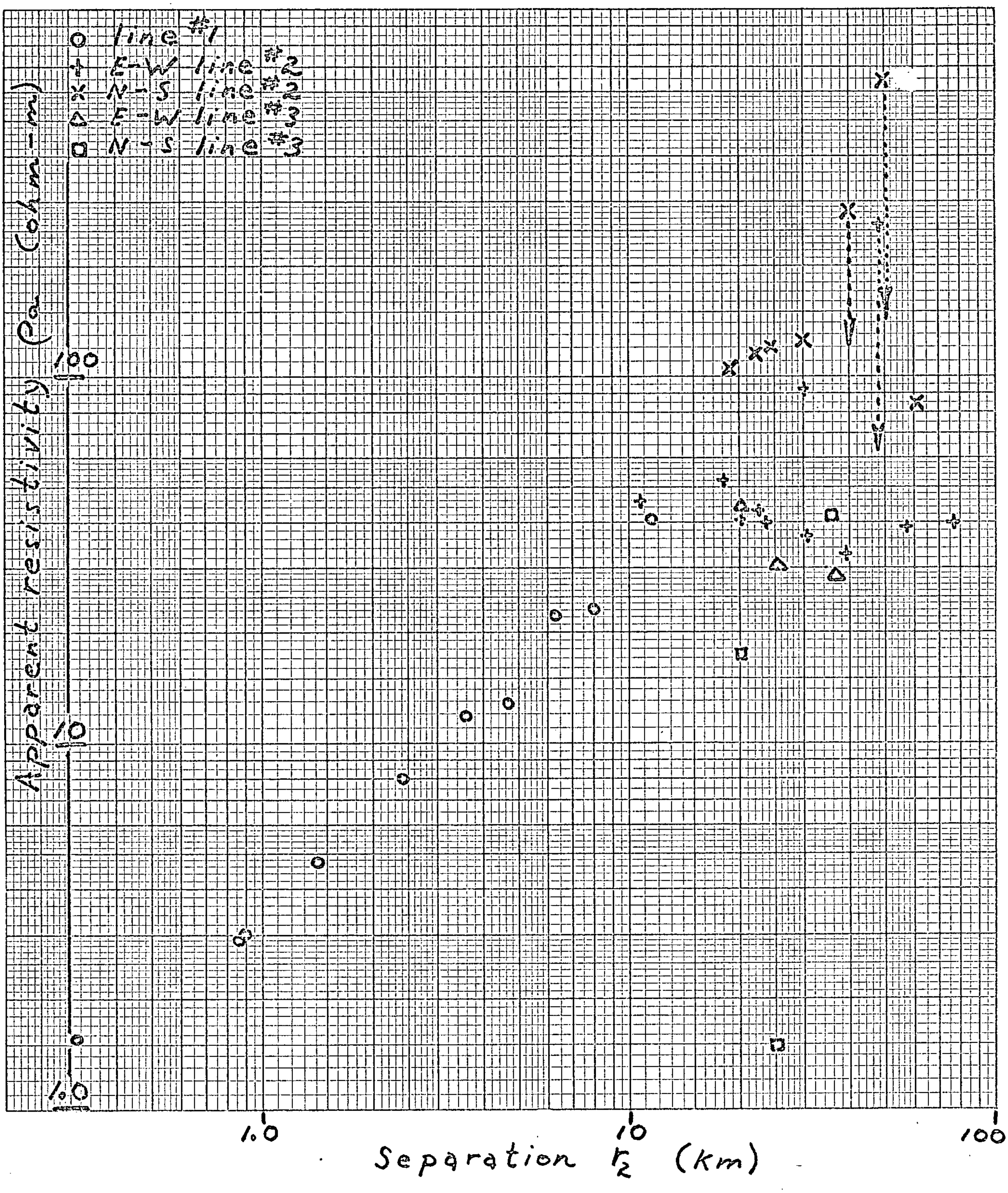

Figure 3-1 Plot of apparent resistivity values.

3-2 Two-Layer Models

3-2-1 Two-Layer Model - Homogeneous Top Layer

For the purposes of initial interpretation, the data can be compared to master curves for a two-layer earth. Figure 3-2 compares two-layer master curves with data from line #1 and east-west arrays on line #2. (All master curves used here are calculated as outlined in Appendix A-3.) The fit of the curves with the data for small r_2 is good, but becomes very poor at large separations, indicating that a more sophisticated model is needed. The maximum slope of a line drawn through the data points is 45°, suggesting a contrast of at least 200 ohm-m between upper and lower layer resistivities. The thickness of the upper layer of Quaternary sediments is estimated to be 500 m but this value is extremely susceptible to variations in the resistivity of the upper layer. Varying the resistivity of the upper layer from 1.0 ohm-m to 2.0 ohm-m varies the interpreted thickness from 300 to 700 m. No consideration has been given to the effects of anisotropic resistivities in the upper layer as these effects should be negligible (see Appendix A-4).

3-2-2 Effect of the Ocean on Two-Layer Models

Before using more sophisticated earth models in interpretation of data, it is first necessary to evaluate the effect of the conductive ocean on layered-earth sounding

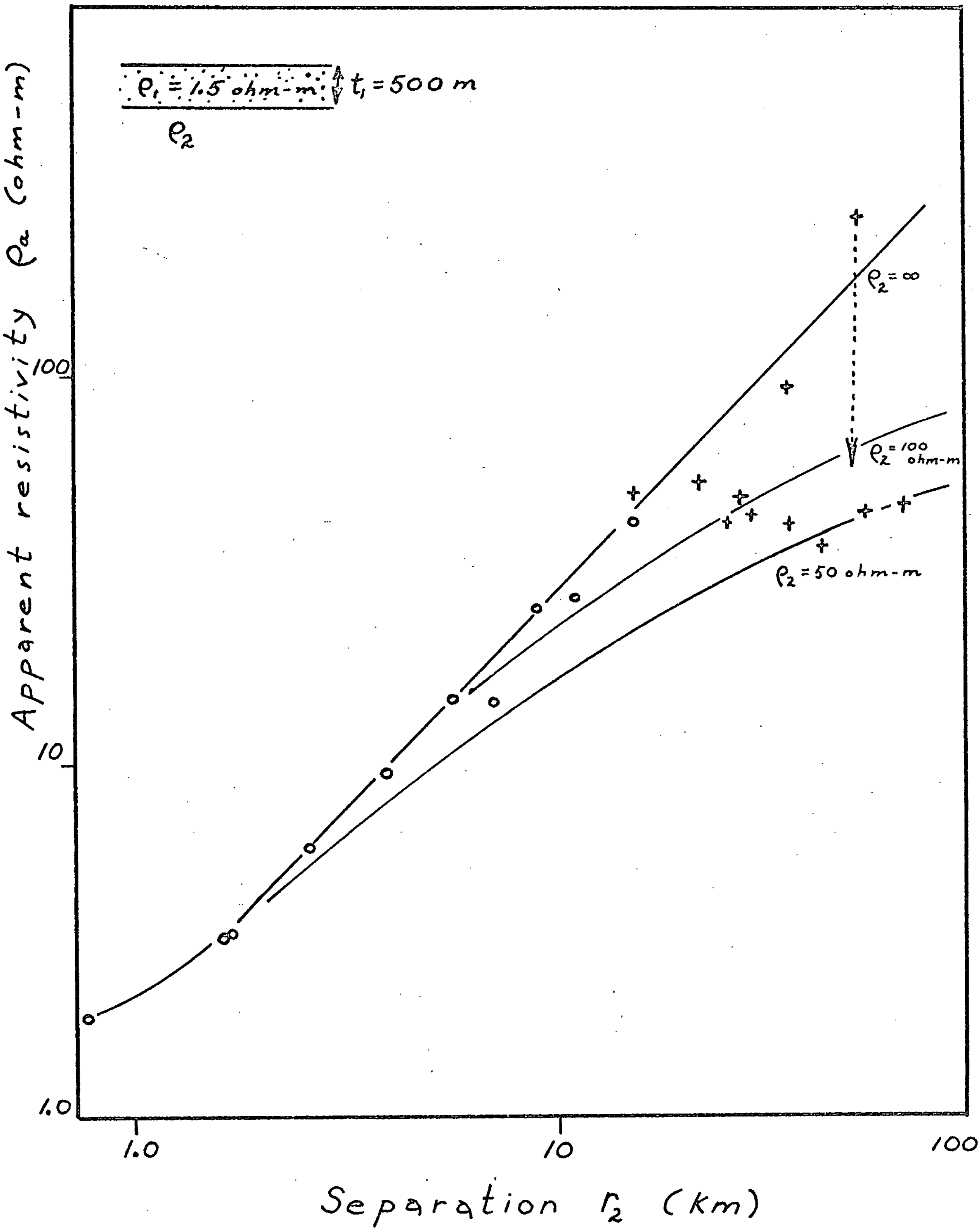

Figure 3-2 Two-layer curves compared with data from line #1 and east-west dipoles on line #2.

curves. The models, Figure 3-3, were designed to approximate the influence of the ocean.

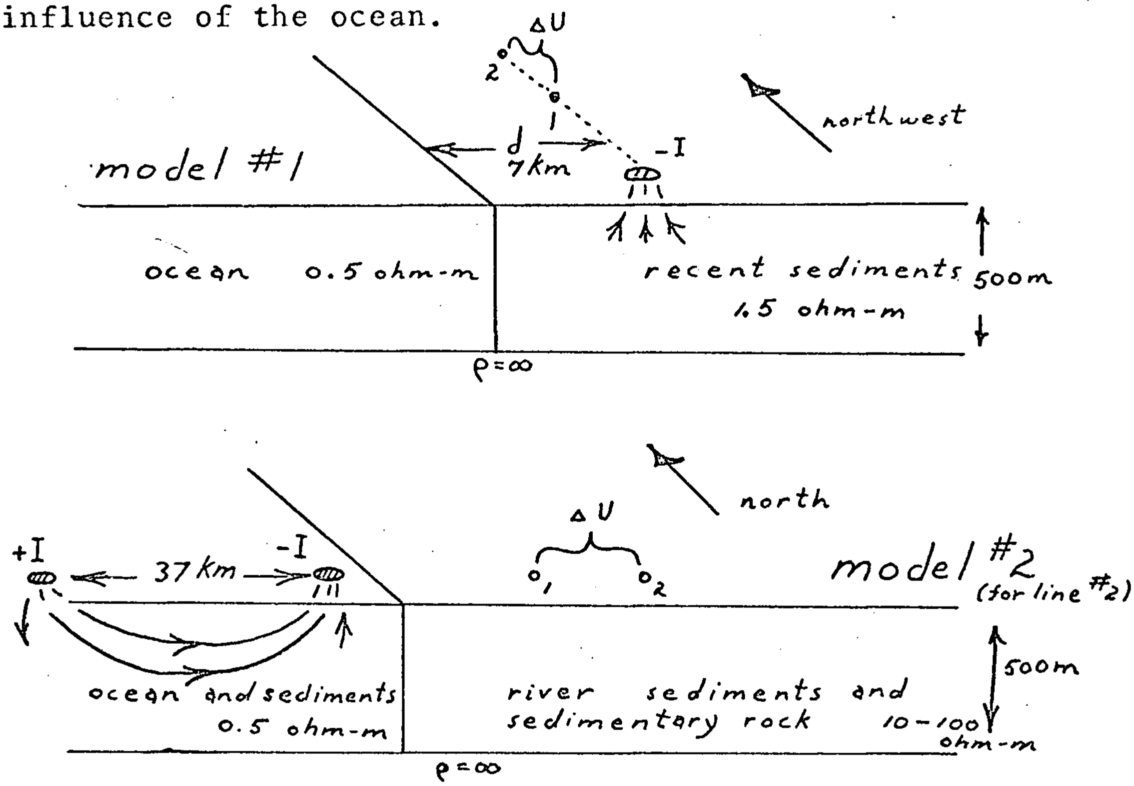

Figure 3-3 Models used in computing sounding curves for an ocean-earth configuration.

Model #1 is used in computing master curves for locations along line #1, running northwest from the cathode. Model #2 is used in computing master curves for locations along line #2, running east from the cathode. (Calculations are outlined in Appendix A-3.) In Figure 3-4 the computed values for these models are compared with the master curves for a two-layer earth. Evidently the curves are almost equivalent *for the range of separations used in this survey.*

On the basis of the above considerations, it will be assumed that the ocean causes little variation in the sounding curves for a layered earth, and that despite the position of the ocean, layered-earth models can be used in approximating resistivities at depth.

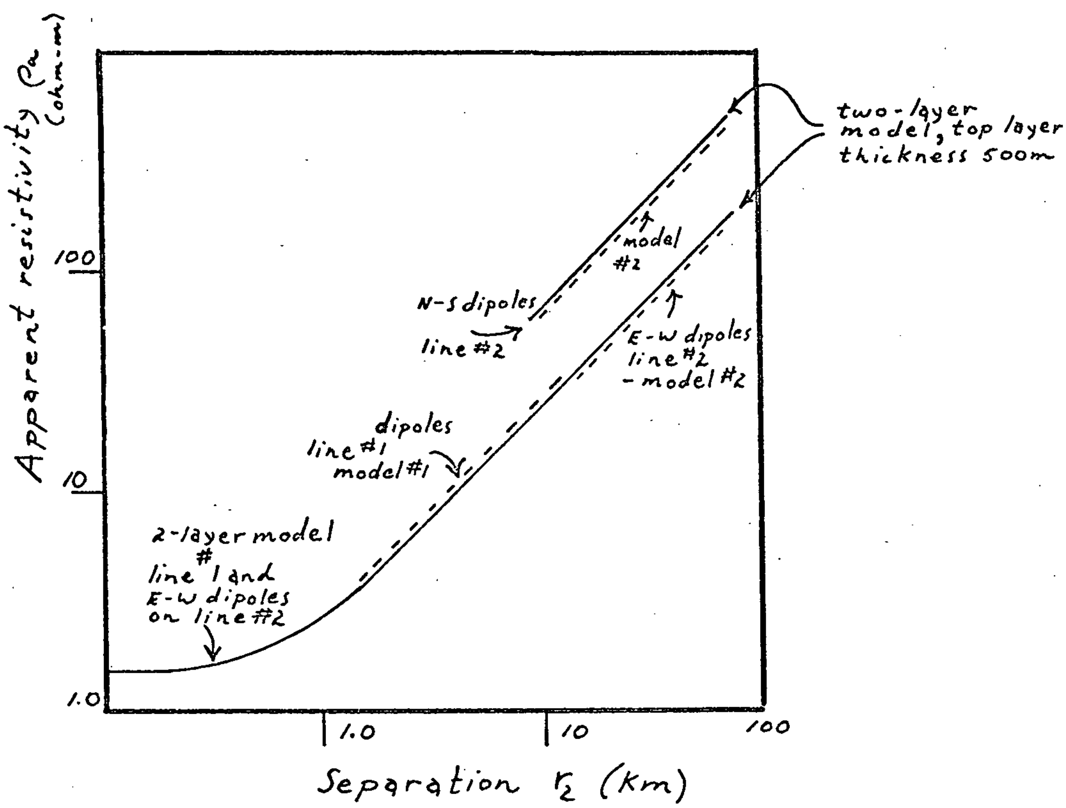

Figure 3-4 Comparison of two-layer sounding curves for homogeneous and inhomogeneous upper layers.

3-3 Three-Layer Models

A final interpretation on the basis of resistivity data alone is limited by the scatter of data points to a three-layer model, Figures 3-5, 3-6, 3-7. The data points for line #1 and east-west dipoles on line #2, Figure 3-5, indicate that the second layer has a transverse resistance[1] (resistivity x thickness) of 1.0×10^6 ohm-m^2 to 2.0×10^6 ohm-m^2 and a minimum resistivity of 200 ohm-m. (Resistivities smaller than this will give a positive slope of less than 45°.) The resistivity of the third layer is probably less than 20 ohm-m. Assuming the minimum value for the resistivity of the second layer would give 10 km as the maximum thickness of the layer.

The data for the north-south dipoles on line #2, Figure 3-6, indicates a somewhat greater transverse resistance for the second layer (greater than 5×10^6 ohm-m^2). The slightly higher values for these dipoles may be due to the presence of the Coast Mountains to the north and east. (Qualitative effects may be determined by referring to M. N. Berdichevskii [2].)

---

[1] For values of resistivity greater than 200 ohm-m, the shape of the curve depends only on the transverse resistance of the second layer (see Appendix A-3).

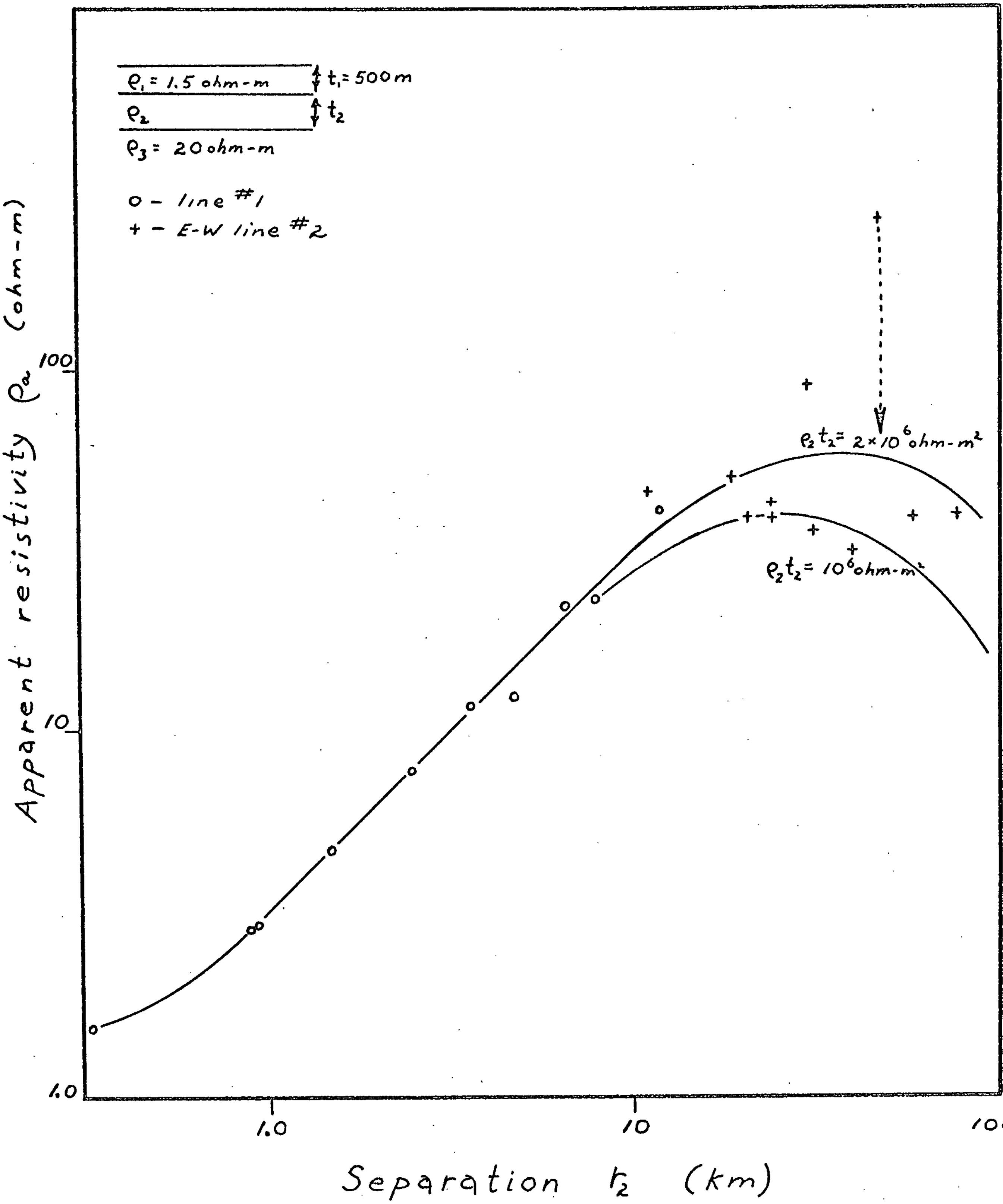

Figure 3-5 Comparison of three-layer model with data from line #1 and east-west dipoles on line #2.

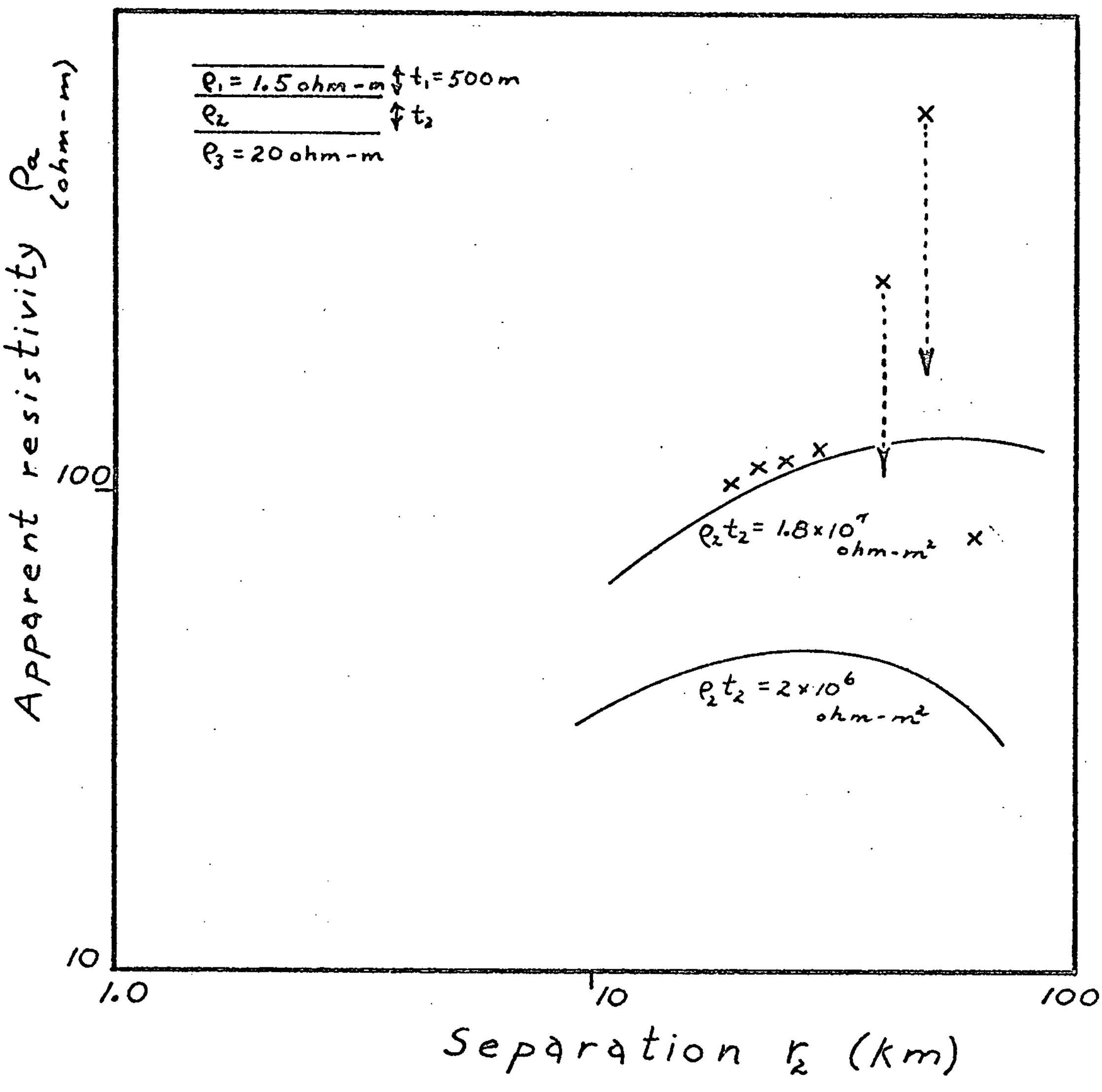

Figure 3-6 Comparison of three-layer model with data from north-south dipoles on line #2.

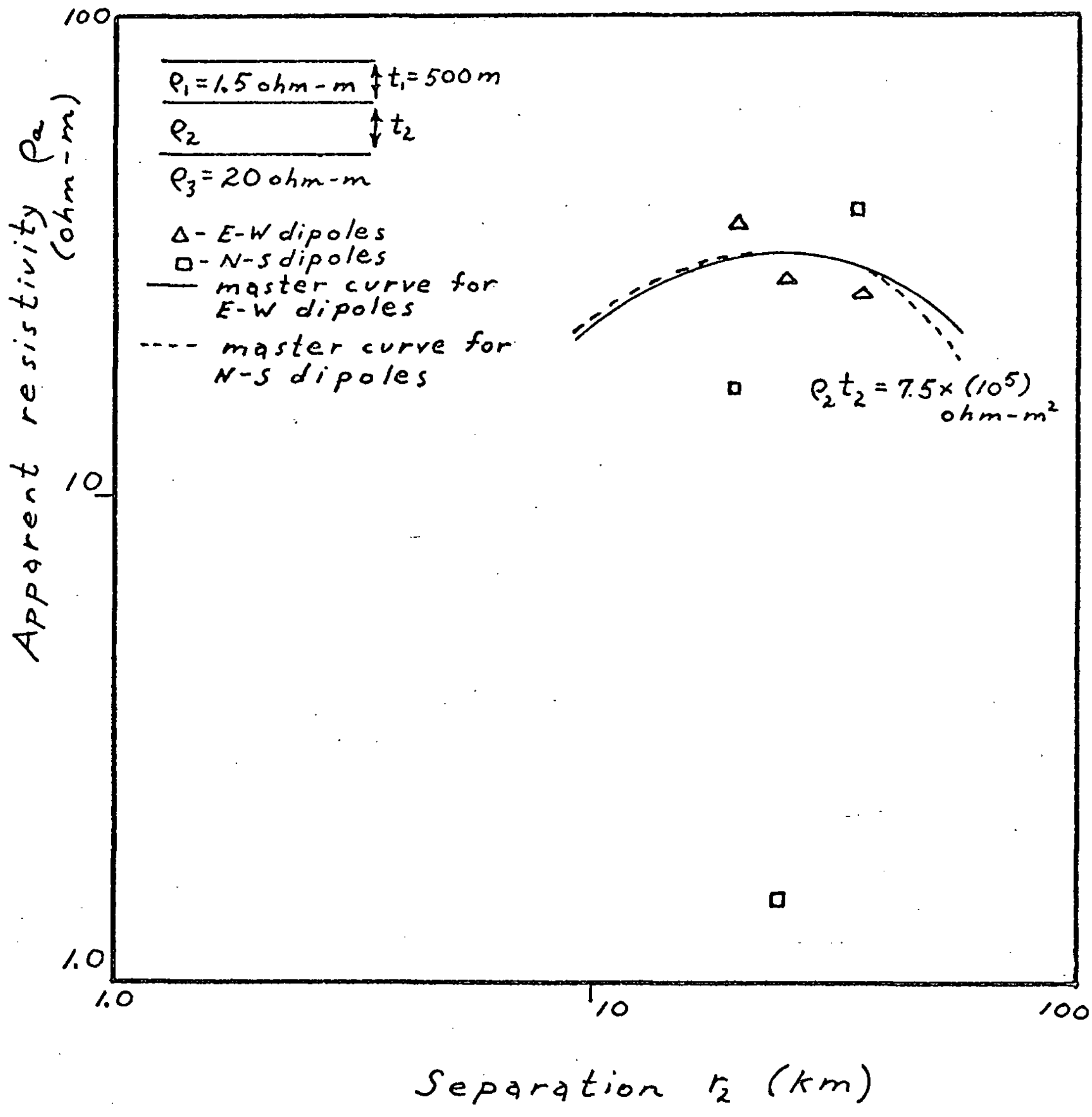

Figure 3-7 Comparison of three-layer model with data from dipoles on line #3.

3-4 Comparison of Resistivity Sounding Data with Seismic and Well Data

A more complex earth model may be designed by comparing resistivity sounding data with seismic and well data. Three deep wells have been drilled in the Fraser Valley area (Richfield Pure Pt. Roberts, Richfield Pure Sunnyside, and Richfield Pure Abbotsford). Induction logs from these wells are represented in Figure 3-8. Values greater than 50 ohm-m tend to be low because induction logging equipment responds poorly to resistive rocks. It is obviously very difficult to set an overall resistivity for the layers of sedimentary rock penetrated by the first two wells. Resistivities here will definitely be anisotropic, having much greater vertical values than horizontal values. (If these resistivity features are widespread, this macro-anisotropy will lead to errors in calculating depths from sounding data - see Appendix A-4.) The Abbotsford well, on the other hand, penetrates a very resistive layer (greater than 300 ohm-m) beginning at 700 m. Considering this well data, a mean resistivity of 200 ohm-m and a minimum depth of 5 km seem reasonable for the layers of sedimentary rock.

One possible interpretation of the resistivity sounding data is that relatively resistant layers of Tertiary and Cretaceous sedimentary rocks overlie a layer of less resistive sedimentary rock. A mean resistivity of 100 to

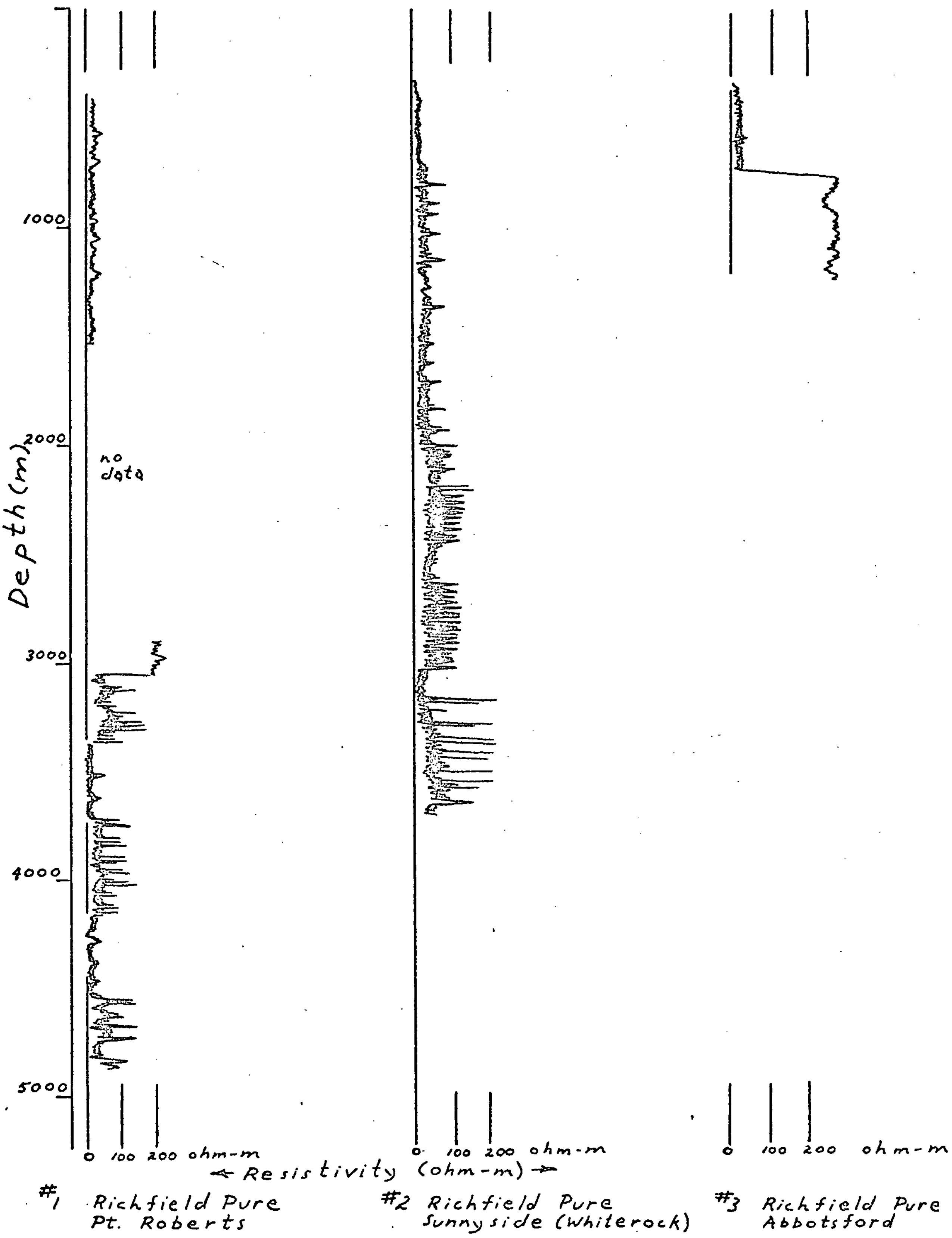

Figure 3-8 Induction logs from wells in the Fraser Valley.

200 ohm-m for the resistive layers would set the upper boundary of the conducting layer at 10 to 20 km. These values are obviously somewhat extreme in view of seismic and geological evidence.

The four-layer model of Figure 3-9 can be composed by assuming that the Tertiary and Cretaceous rocks overlie granitic rocks. The change in resistivity from the granitic to the lower layer need not be discontinuous but can be very gradual. The best fit to data from line #1 and east-west dipoles on line #2 is found when the thickness of the granitic layer is two kilometers (Figure 3-9). For larger resistivities of the granitic layer, this value would be proportionately less. Data from the north-south dipoles of line #2 implies that the thickness is greater than 5 km. As stated before, however, the resistivities measured here may be higher than expected for a layered earth. Figure 3-10 compares the four-layer model deduced from resistivity data with a seismic model of K. H. Tseng [24].

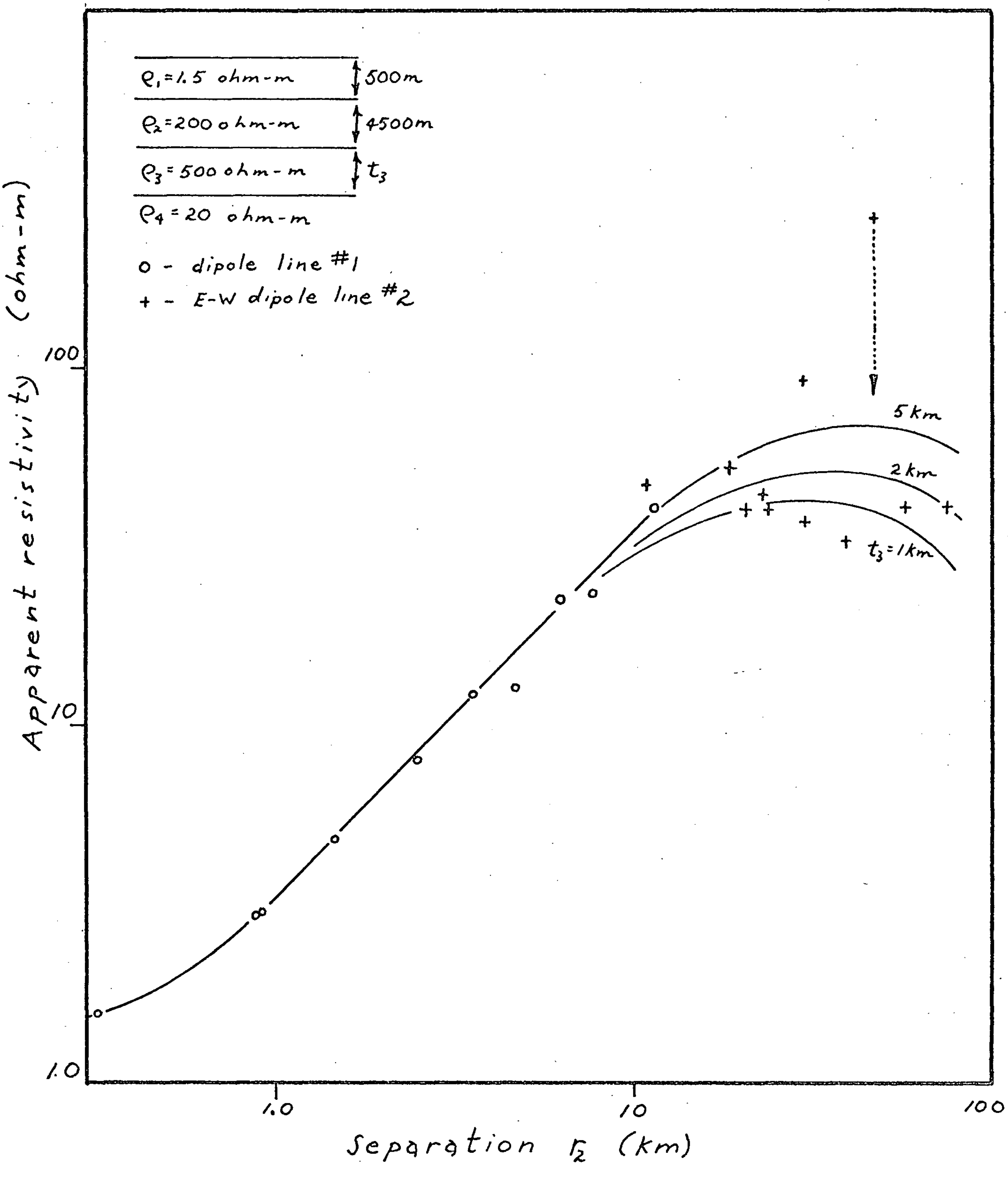

Figure 3-9 Comparison of four-layer model with data from line #1 and east-west dipoles on line #2.

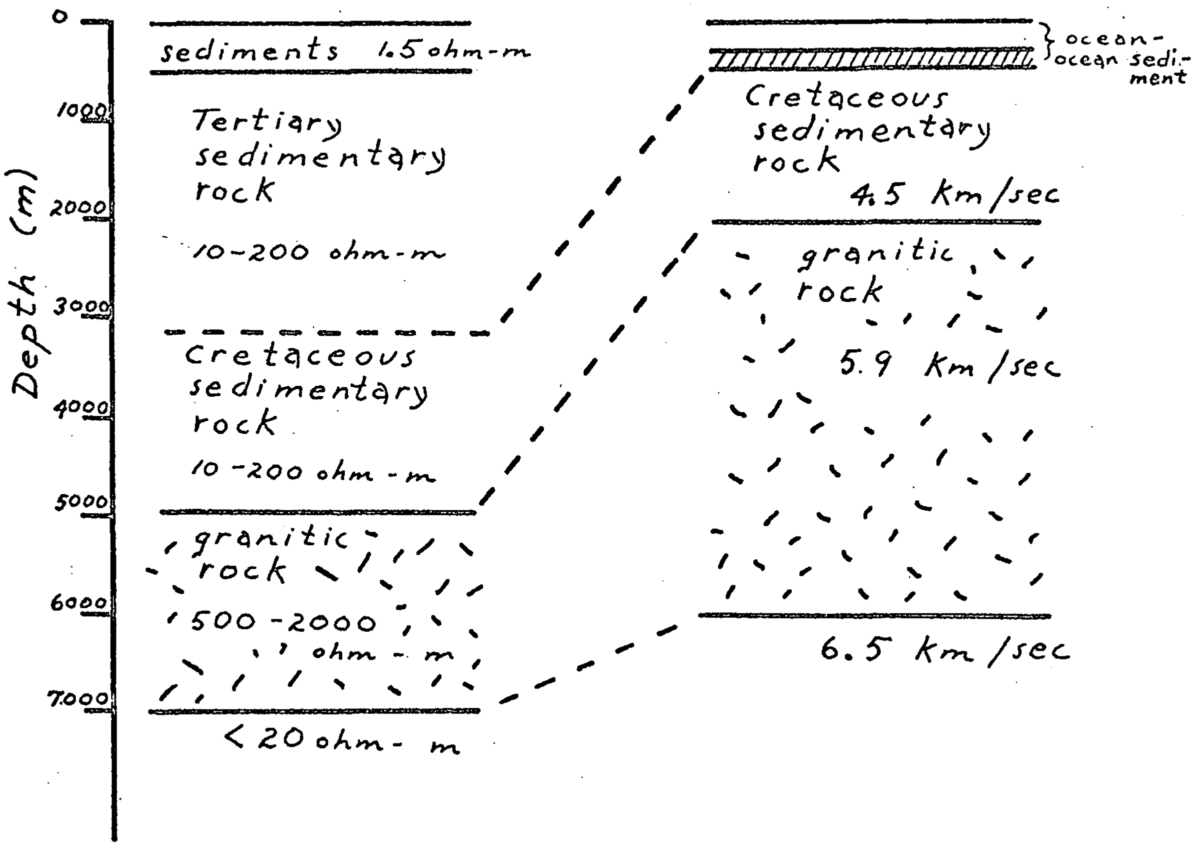

(a) Model for Fraser Valley and Delta from well and resistivity sounding data.

(b) Model for south-west Georgia Strait from seismic data (K. H. Tseng [24]).

Figure 3-10 A comparison of resistivity and seismic profiles near the Fraser Delta.

3-5 Discussion

If the four-layer model of Figure 3-10 is accepted, the conductive layer underlying the granitic rock presents an interesting puzzle. Neither temperature nor hydrostatic pressure could account for such low values of resistivity at 7 - 8 km. The temperature would have to be near 800°C (E. I. Parkhomenko [19]) which is much too high for these depths. Expected values are usually no greater than 300°C.

One possibility is that the increased conductivity is caused by water saturation of the rock. As the partial pressure of water vapour in a rock is increased, the amount of bound or adsorbed water increases accordingly. This increase in water content of the rock aids dissociation and lowers the overall activation energy for ionic conduction in the system. At the high vapour pressures possible at depth, the resistivity of a given rock could be lowered enormously. Figure 3-11 indicates the effects of partial water vapour pressure and temperature on the resistivity of a granite. Unfortunately, for our purposes the temperature range is too high. Resistivities at lower temperatures may be approximated by assuming $\rho \propto \exp(E(P)/T)$ (E. I. Parkomenko [19]) where T is absolute temperature and E is activation energy, a function of partial vapour pressure P. Choosing suitable values for pressure and temperature as a function of depth, and assuming that the vapour pressure is equal

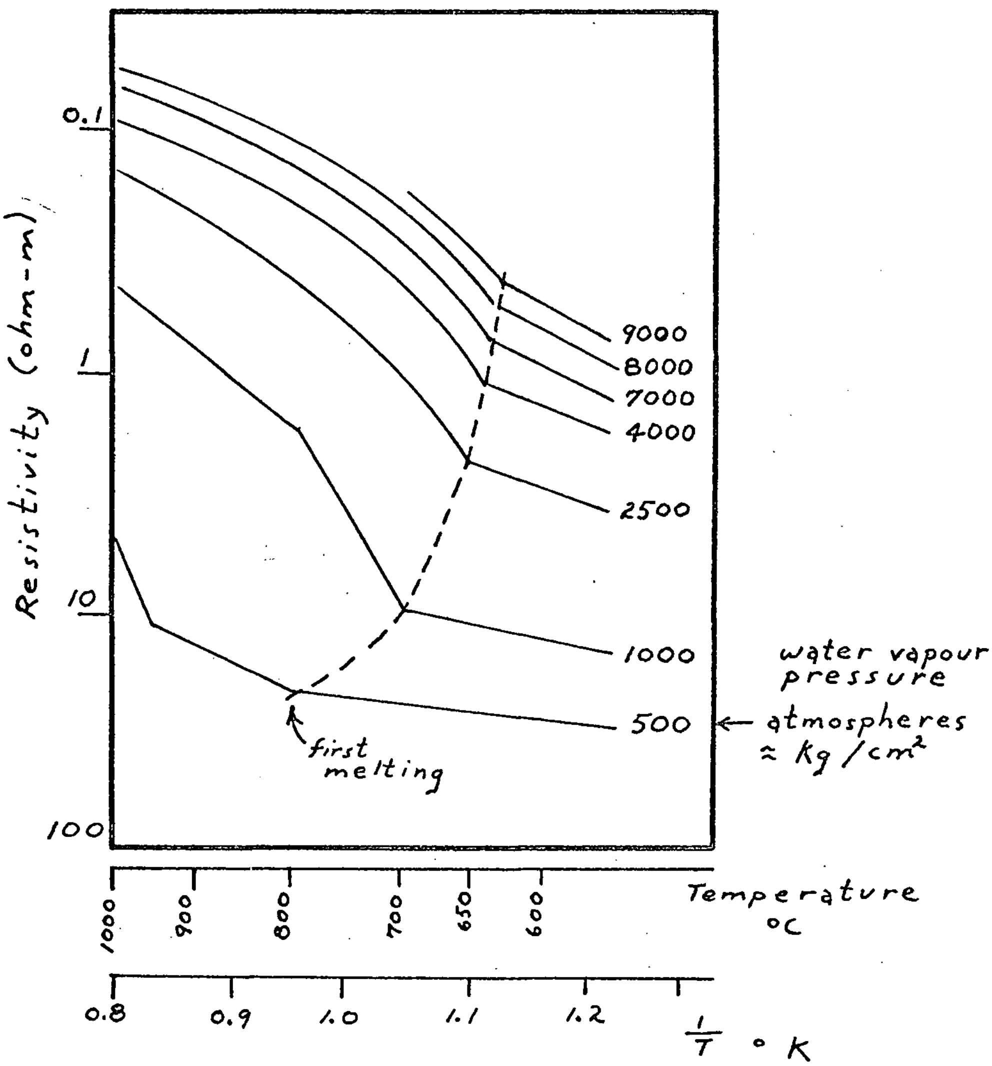

Figure 3-11 Resistivity of a granite as a function of temperature and water vapour pressure. (From E. B. Lebedev and N. I. Khitarov [16]).

to the hydrostatic pressure gives the resistivity values of Figure 3-12.

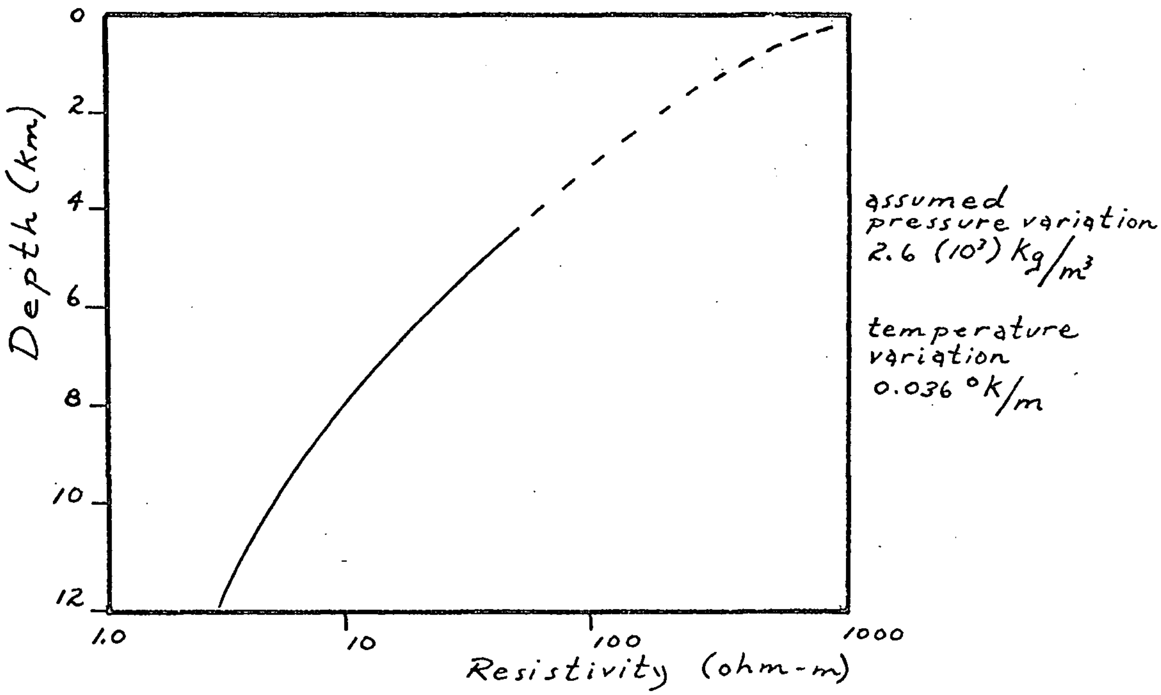

Figure 3-12 Resistivity of a water saturated granite as a function of depth.

Clearly the values at 8 km compare favourably with measured resistivities.

An interesting feature is that the resistivities at greater than 15 km are approximately those found from geomagnetic depth soundings (Caner et al [5]).

Large amounts of water in metamorphic rocks would be a direct consequence of the rock's sedimentary origin. Deformation and thickening of geosynclinal sediments, followed by continued high radioactive heat production would cause partial melting to occur at the base of the sediments. Granitic melts, with high water content, would slowly rise toward the surface. Thus, in young orogenic regions, one expects a near surface layer that is largely granitic over a water-saturated layer of intermediate composition (granitic rocks and amphibolites). The seismic velocity of such a mixture would be approximately 6.5 km/sec (A.E. Ringwood and D. H. Green [20]) which agrees well with seismic data for this region (Figure 3-10 b). The Potassium-Argon age, mid-Miocene, assigned to granitic rocks near Chilliwack (J. A. Roddick [21]) also agrees well with the above considerations.

Other shallow, conductive anomalies (less than 20 km deep) in areas with granitic basements, Figure 3-13, may be the result of equivalent processes. (A more complete description of the mechanisms involved is given by R. D. Hyndman and D. W. Hyndman [10].)

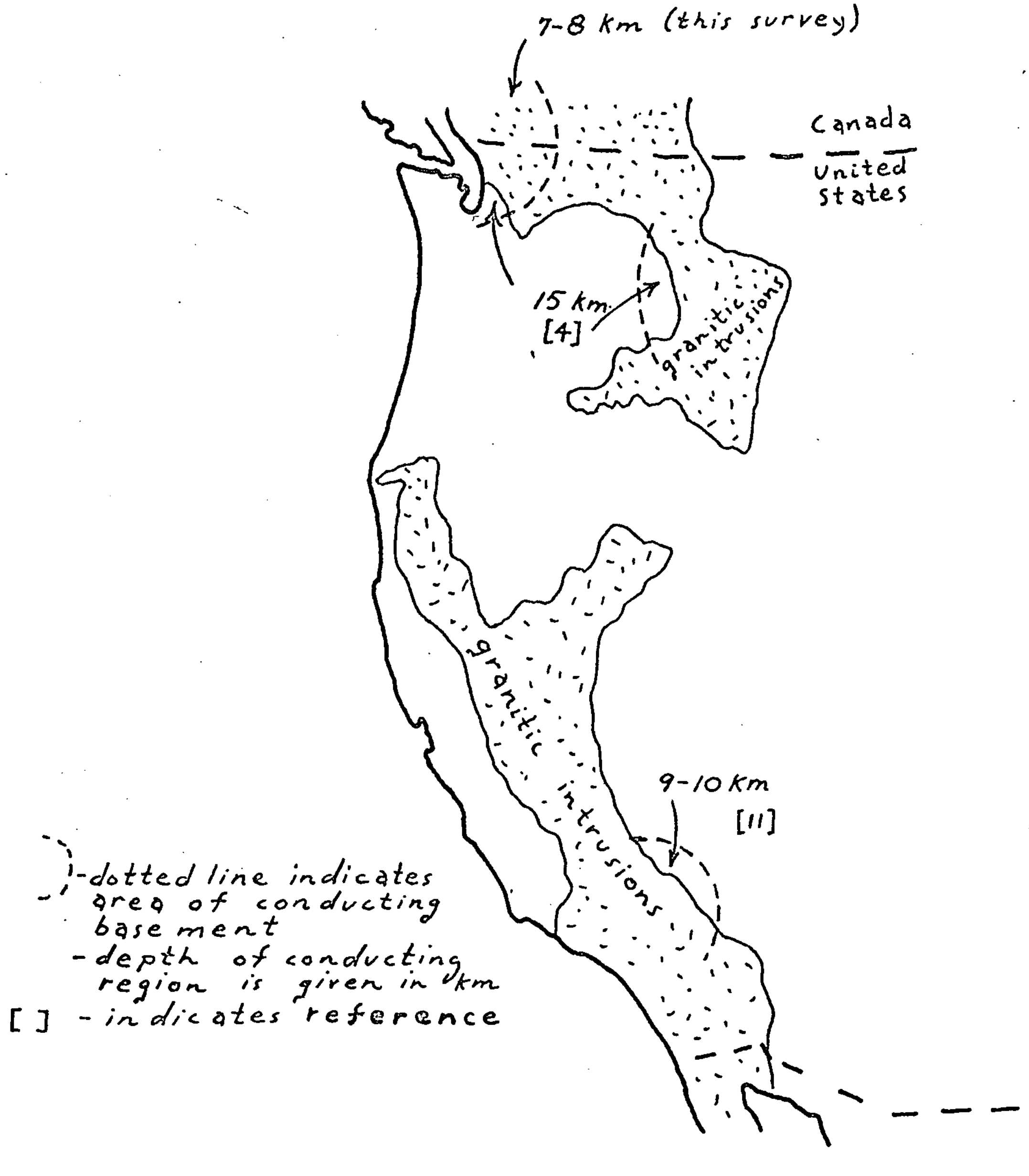

Figure 3-13 Shallow conducting anomalies in western North America.

4 CONCLUSIONS

It is obvious that a layered earth model gives the best fit to the resistivity sounding data. Calculations have shown that the conductive ocean has an insignificant effect on simple two-layer potentials and probably has little effect on multilayered models. It is inconceivable that other lateral variations in resistivity could give values which compare with the data for all the dipole orientations used in this survey. Scatter of data points is small enough to permit a three-layer interpretation.

The sounding data combined with well data allows a four-layer interpretation in which 500 m of conductive Quaternary sediments overlie 4-5 km of Tertiary and Cretaceous sedimentary rocks and 2 km of resistive granitic rocks. The interpreted thickness of the granitic rocks depends very much on the assumed resistivities of the sedimentary and granitic rocks. If the resistivity of the granitic rock declines as rapidly as is indicated in Figure 3-12, the thickness might be closer to the 4-5 km value deduced from seismic data in southern Georgia Strait.

The conducting region below the granitic rocks is probably the upper part of the layer found using geomagnetic depth soundings. The relatively shallow depth and the low resistivity (<20 ohm-m) make it improbable that the effects are caused by high temperatures. High conductivity of the rocks in this region could be the result of increased dissociation and ionic mobility in water saturated rocks. Other shallow conducting anomalies in western North America may be manifestations of this phenomenon.

SUGGESTIONS FOR FURTHER STUDY

Much valuable information could be obtained by extending the line of potential measurements along the Fraser Valley. B.C.H.P.A. plans to pulse a 1200 amp current through the input dipole which should allow measurements to be made at dipole spacings of up to 150 km. This would make it possible to set a representative resistivity and a minimum thickness for the conducting layer underlying the granitic rocks.

Maximum dipole separations would be obtained by orienting the measuring electrodes in the expected direction of the electric field. Great care should be taken to use a common orientation at all measuring locations as random orientations can lead to large changes in apparent resistivity (G. V. Keller [14]). In any case, scatter of data would probably be large because of the relatively complex surface features of the eastern Fraser Valley.

If possible, the lateral extent of the resistivity soundings should be increased by making potential measurements on Vancouver Island. This area has the added advantage that a large amount of seismic information is available (W. R. H. White and J. C. Savage [26]). The best locations for measuring dipoles are on a line following the eastern coast of the island. The surface here is a relatively uniform layer of Cretaceous sedimentary rocks whereas geology on most other parts of the island is very complex (R. I. Walcott [25] p. 11). Maximum dipole separations on this line will probably not be so great as those along the Fraser Valley because of the increased telluric noise in the more resistive Cretaceous rocks.

REFERENCES

[1] Berdichevskii, M. N., 1965, Electrical prospecting with the telluric current method: Colorado School of Mines Quat., v. 60, 216 p.

[2] Berdichevskii, M. N. and Zagarmistr, A. M., 1966, Methods of interpreting dipole resistivity soundings, *in* Dipole methods for measuring earth conductivity: New York, Consultants Bur., p. 79-112.

[3] Caner, B., Cannon, W. H., and Livingstone, C. E., 1967, Geomagnetic depth sounding and upper mantle structure in the Cordillera region of western North America: Jour. Geophys. Res., v. 72, p. 6335-6351.

[4] Cantwell, T., Nelson, P., Webb, J., and Orange, A. S., 1965, Deep resistivity measurements in the Pacific northwest: Jour. Geophys. Res., v. 70, p. 1931-1937.

[5] Cantwell, T., and Orange, A. S., 1965, Further deep resistivity measurements in the Pacific northwest: Jour. Geophys. Res., v. 70, p. 4068-4072.

[6] Cooley, J. W., Lewis, P. A. W., and Welch, P. D., 1967, Application of the Fast Fourier Transform to computation of Fourier integrals, Fourier series, and convolution integrals: I.E.E.E. Transactions On Audio and Electroacoustics, v. AU-15, p. 79-84.

[7] Flathe, H., 1955, A practical method of calculating geoelectrical model graphs for horizontally stratified media: Geophys. Prosp., v. 3, p. 269-294.

[8] Grant, F. S., and West, G. F., 1965, Interpretation theory in applied geophysics: New York, McGraw-Hill.

[9] Hopkins, W. S., 1966, Palynology of Tertiary rocks of the Whatcom Basin, southwestern British Columbia and northern Washington: Unpublished Ph.D. thesis, Dept. of Geology, University of British Columbia.

[10] Hyndman, R. D., and Hyndman D. W., 1968, Water saturation and high electrical conductivity in the lower continental crust: Manuscript of paper given at Can. Assoc. of Phys. convention, Calgary, Alberta, Canada, 1968.

[11] Jackson, D. B., 1966, Deep resistivity probes in the southwestern United States: Geophysics, v. 31, p. 1123-1144.

[12] Keller, G. V., and Frischknecht, F. C., 1966, Electrical methods in geophysical prospecting: New York, Pergamon Press.

[13] Keller, G. V., 1966, Dipole methods for measuring earth conductivity, *translation from Russian:* New York, Consultants Bur.

[14] Keller, G. V., 1966, Dipole method for deep resistivity studies: Geophysics, v. 31, p. 1088-1104.

[15] Lahman, H. S., and Vozoff, K., 1965, Deep resistivity results from D. C. ground tests at Hoover Dam: Geoscience Inc., Scientific Report 6.

[16] Lebedev, E. B., and Khitarov, N. I., 1964, Dependence of the beginning of melting of granite and the electrical conductivity of its melt on high water vapour pressure: Geochem. Int., v. 1, p. 193-197.

[17] Misch, P., 1966, Tectonic evolution of the northern Cascades of Washington State, *in* Tectonic history and mineral deposits of the western Cordillera: Canadian Inst. of Mining and Metallurgy, Special v. 8, p. 101-149.

[18] Mooney, H. M., Orellana, E., Pickett, H., and Tornheim, L., 1966, A resistivity computation method for layered earth models: Geophysics, v. 31, p. 192-203.

[19] Parkhomenko, E. I., 1967, Electrical properties of rocks: New York, Plenum Press.

[20] Ringwood, A. E., and Green, D. H., 1966, Petrological nature of the stable continental crust, *in* The earth beneath the continents: Richmond, William Byrd Press.

[21] Roddick, J. A., 1966, Coast crystalline belt of British Columbia, *in* Tectonic history and mineral deposits of the western Cordillera: Canadian Inst. of Mining and Metallurgy, Special v. 8, p. 73-82.

[22] Stefanescu, S. S., and Schlumberger, C. and M., 1930, Sur la distribution électrique potentielle autour d'une prise de terre ponctuelle dans un terrain à couches horizontales, homogènes et isotropes: Jour. Physique et le Radium, v. 1, p. 132-140.

[23] Sunde, E., 1949, Earth conduction effects in transmission systems: New York, Van Nostrand Co.

[24] Tseng,K.H., 1968, A new model for the crust in the vicinity of Vancouver Island: Unpublished M.Sc. thesis, Dept. of Geophysics, University of British Columbia.

[25] Walcott, R. I., 1967, The Bouguer anomaly map of southwestern British Columbia: University of British Columbia Inst. of Earth Sciences, Scientific Report 15, p. 32.

[26] White, W. R. H., and Savage, J. C., 1965, A seismic refraction and gravity study of the earth's crust in British Columbia: Bull. Seis. Soc. Am., V.55, p. 463-486.

APPENDIX

A-1 Equipment

(a) Characteristics of Astrodata TDA-121 Nanovoltmeter (5)

1 AMPLIFIER GAIN ACCURACY - ±1%

2 BAND WIDTH - down 3 db at 0.2 Hz

3 INPUT IMPEDANCE - 1 megohm

4 GROUND ISOLATION - entire circuit is floating from panel and cabinet by at least 1000 megohms resistance and not more than 0.01 mf capacitance

(b) Characteristics of Brush 280-10 Recorder (6)

1 INPUT IMPEDANCE - 1 megohm

2 LINEARITY- 0.25% full scale

3 REPEATABILITY - 0.1%

4 FREQUENCY RESPONSE - less than 2% amplitude distortion full scale for frequencies less than 20 Hz

5 GROUND ISOLATION - circuit is floating from cabinet at no less than 1 megohm

(c)

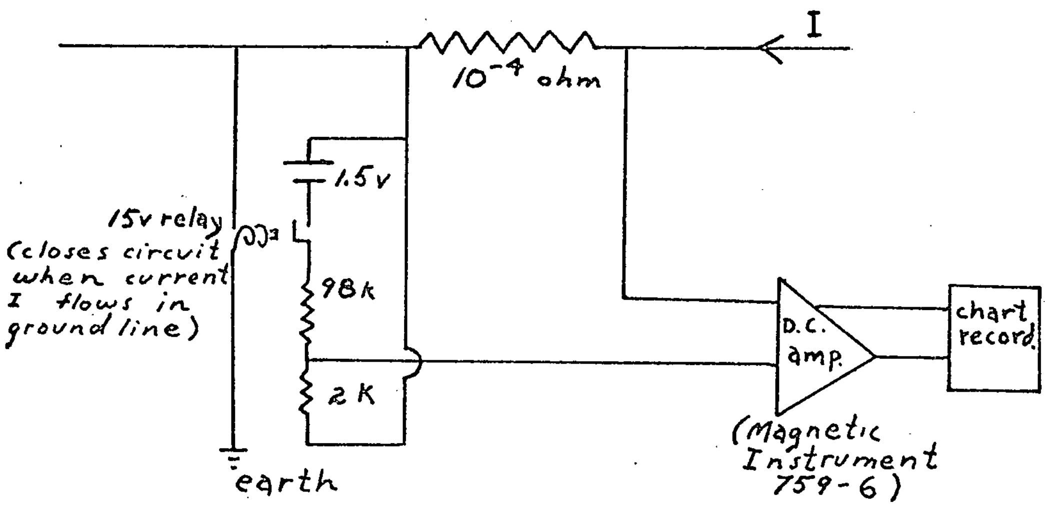

Figure A-1 Input monitor.

(d)

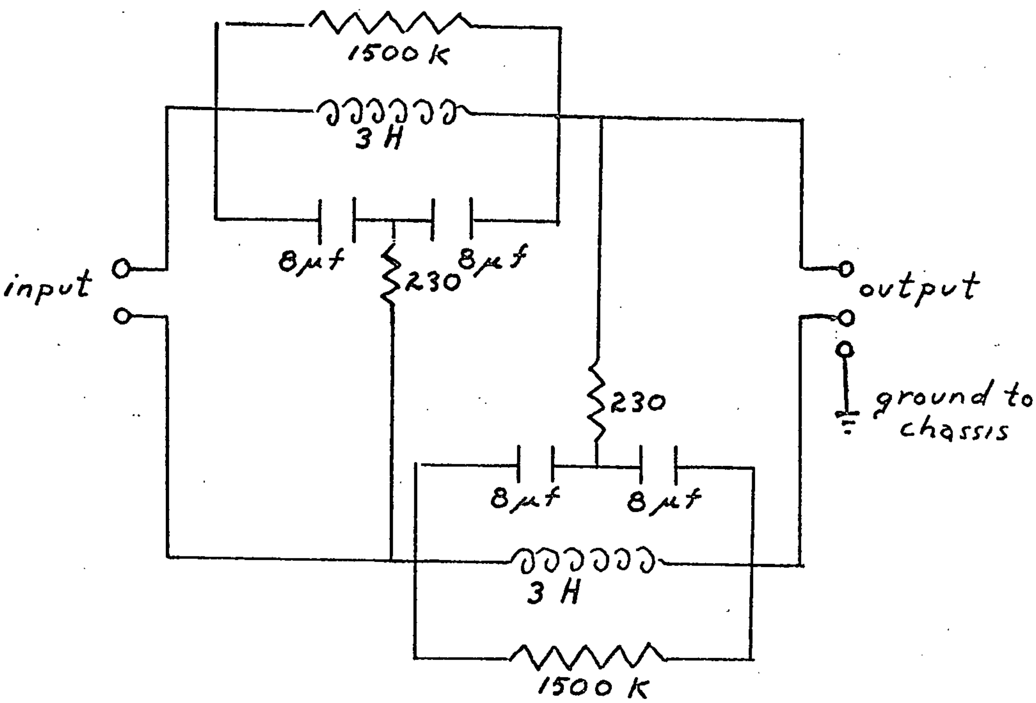

Figure A-2 60 Hz filter.

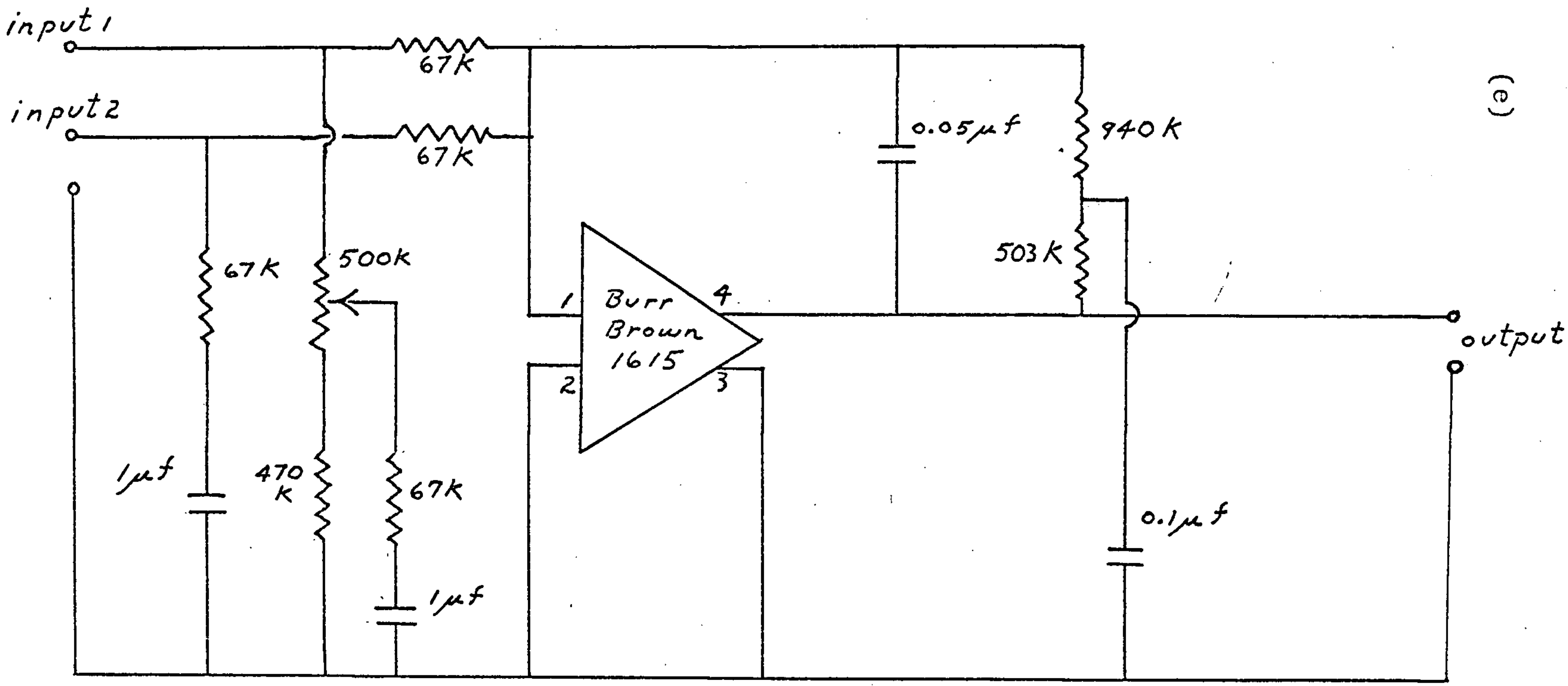

<u>Characteristics</u>

GAIN
  Channel 1   5-10
  Channel 2   10

CUTOFF
  1 Hz
  12 db/octave

Figure A-3 Summing amplifier.

A-2 Estimation of Signal Amplitudes in Noisy Records

At large dipole separations the signal was often obscured by noise. Consequently, signal amplitudes could not be estimated by visual inspection of recorded data. In these cases, the amplitude of the signal was estimated from the amplitudes of its first four harmonics.

For finite record lengths, the Fast Fourier transform may be used to find a Fourier series of the form

$$F(t) \approx \sum_{n=1}^{N/2} (A_n \cos n\,\omega t + B_n \sin n\,\omega t) \qquad \text{(A-1)}$$

(J. W. Cooley et al [6])

(All records have an integral number of input signal cycles.)

t is time;

N is the number of sample points;

$\omega = 2\pi/T$, T is the sample length;

$A_n = a_n + \overline{a_n}$, a_n is the signal amplitude;

$\overline{a_n}$ is the noise amplitude

$B_n = b_n + \overline{b_n}$, b_n is the signal amplitude;

$\overline{b_n}$ is the noise amplitude;

$a_n, b_n = 0$ if $n \neq \ell \times t$ $(\ell = 1, 2, 3 \ldots)$,

t is the number of signal cycles in the sample space

The amplitude of the signal may be estimated by matching the square of the amplitude spectrums of signals of known amplitudes $C^2_{\ell t}$ with the square of the amplitude spectrum of the record, such that one minimizes

$$\sum_{\ell} \left|(A_{\ell t}^2 + B_{\ell t}^2) - C_{\ell t}^2\right| \qquad \text{(A-2)}$$

The square of the amplitude spectrum is used as, in general, the phase of the input signal is not known. [1] Matching four harmonics was assumed to give sufficient accuracy. An example of the matching and the resultant signal form are shown in Figures A-4 and A-5 respectively.

Application of this method to synthetic noisy records, where the signal amplitude was known, indicated a probable error of no more than 20% for a signal-to-noise ratio[2] of 0.1.

---

[1] It is possible, in some cases, to use only the amplitude of the fundamental in determining signal values. This can, however, lead to sizeable errors at other times. The natural telluric noise at the fundamental frequency may be quite large even though noise value at other frequencies are insignificant.

[2] Background potentials were considered noise only at frequencies greater than .02 Hz. Presence of these high frequencies makes it difficult to detect ON and OFF changes for the signal. The *signal-to-noise* ratio is defined as

$$(\text{Peak Amplitude of signal})^2/(\text{Amplitude of Dominant Frequency of Noise})^2$$

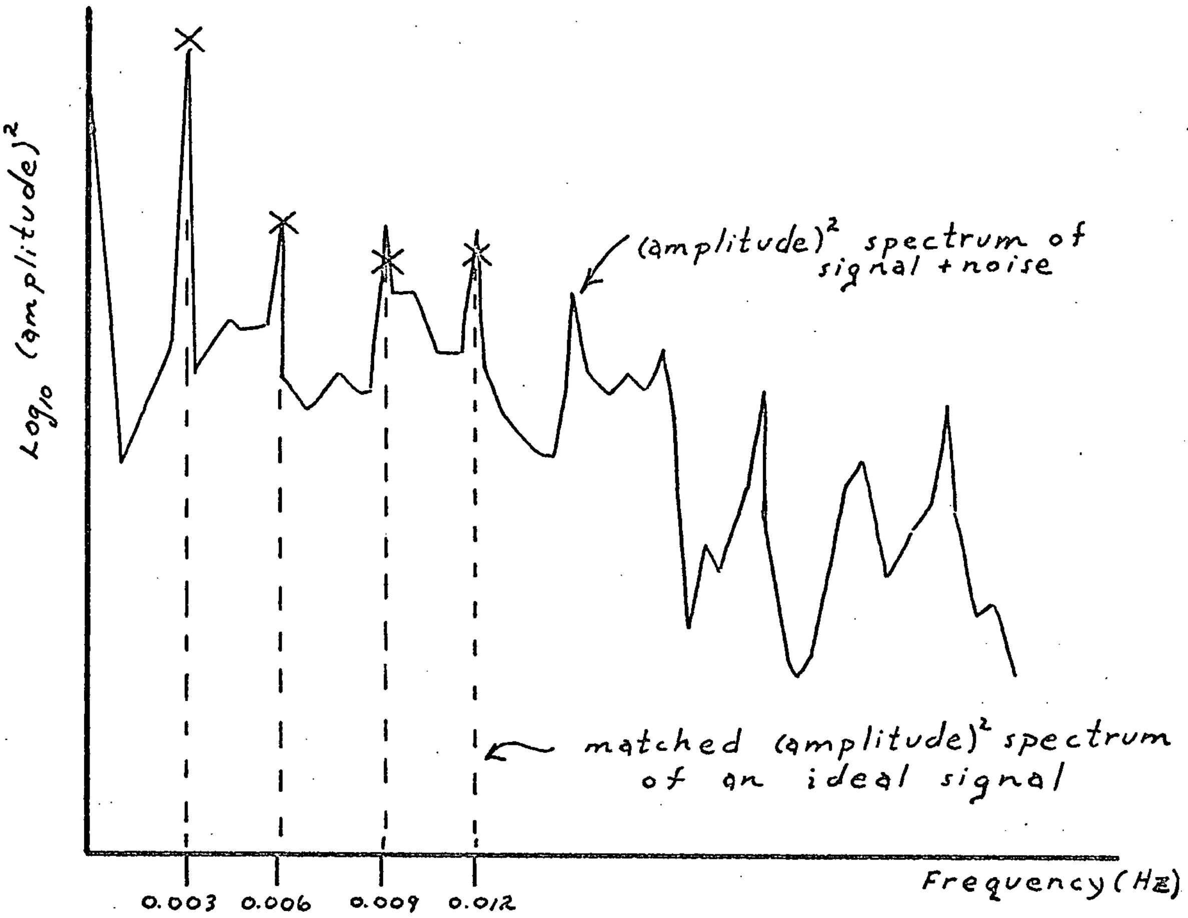

Figure A-4 Square of amplitude spectrums of signal and noise.

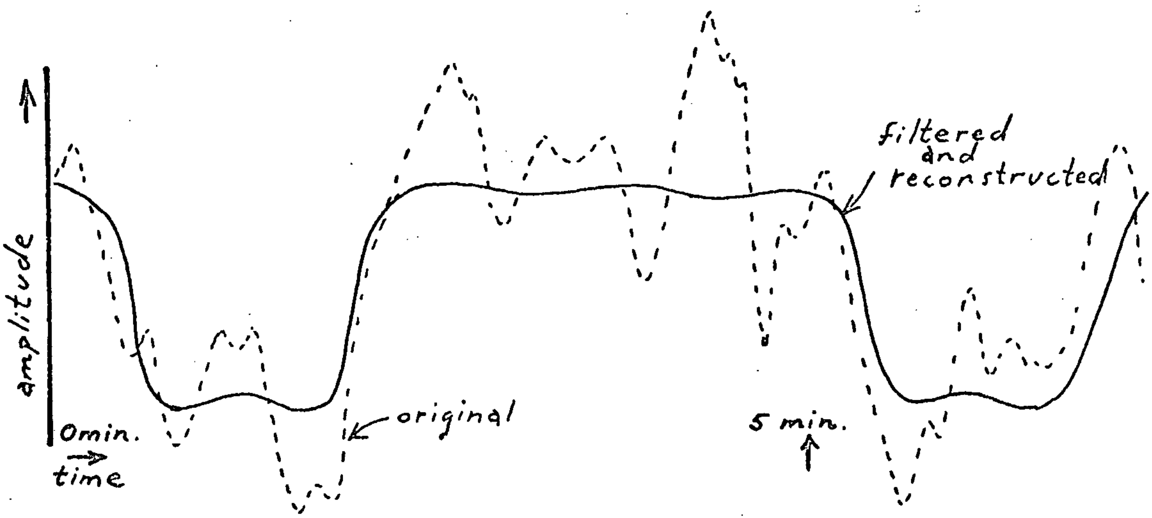

Figure A-5 Reconstructed signal compared to original.

A-3 Calculation of Master Curves

As no master curves were available for the particular dipole configurations used in this survey, methods for computing these curves were devised. The following pages outline the computations.

A-3-1 Two-Layer Model - Inhomogeneous Top Layer

Surface potentials for models #1 and #2, page 37 were calculated by using the method of images to replace the boundary in the upper layer by a point source. The image method is based on the assumption that, in most aspects, electric currents behave like light rays. A boundary, Figure A-6, may be considered a mirror with reflection coefficient

$$K_{1,2} = \frac{\rho_2 - \rho_1}{\rho_2 + \rho_1}$$

and transmission coefficient $1 - K_{1,2}$ (see G. V. Keller and F. C. Frischknecht [12]).

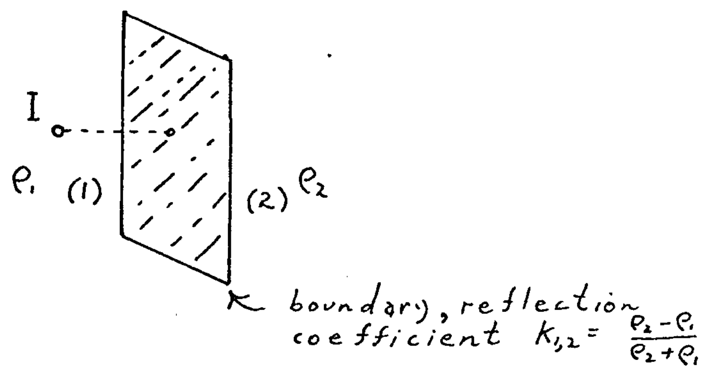

Figure A-6 A resistive boundary.

Values of the potential U in medium 1, Figure A-7, are found by replacing the vertical boundary by a source $K_{1,2}I$ a distance d behind the position of the boundary.

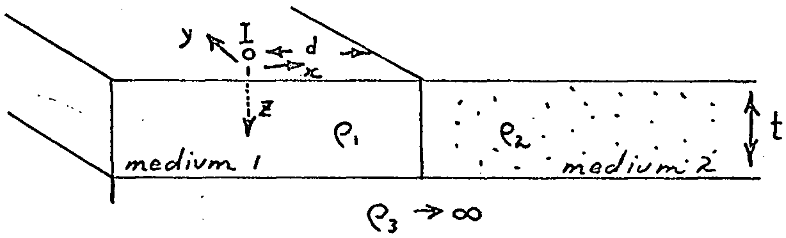

Figure A-7 Overburden with a lateral change in resistivity.

The validity of the step can be established by considering the equivalence of path 1 and 2 in Figure A-8 when $\rho_3 \to \infty$ and $K_{1,3} \to K_{2,3}$.

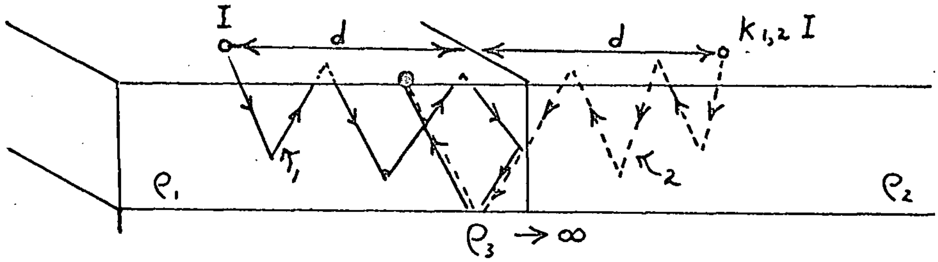

Figure A-8 Replacement of a boundary by a point source.

For one source I in an overburden

$$U = \frac{\rho_1 I}{2\pi}\left[\frac{1}{r} + 2\sum_{n=1}^{\infty}\frac{K_{1,3}^{n}}{[r^2 + 4n^2t^2]^{\frac{1}{2}}}\right] \qquad \text{(A-4)}$$

where U is a potential on the surface, $r = (x^2 + y^2)^{\frac{1}{2}}$.

(G. V. Keller et al [12])

Thus for two sources, I and $K_{1,2}I$

$$U_1 = \frac{\rho_1 I}{2\pi}\left[\frac{1}{r} + \frac{K_{1,2}}{((2d - x)^2 + y^2)^{\frac{1}{2}}}\right.$$

$$\left. + 2\sum_{n=1}^{\infty}\left\{\frac{K_{1,3}^{n}}{(r^2 + 4n^2t^2)^{\frac{1}{2}}} + \frac{K_{1,3}^{n}\,K_{1,2}}{((2d - x)^2 + y^2 + 4n^2t^2)^{\frac{1}{2}}}\right\}\right] \tag{A-5}$$

$$K_{1,3} \rightarrow 1$$

To find potentials in medium 2 the source I is replaced by a source $(1 - K_{1,2})I$

$$U_2 = \frac{\rho_2 I}{2\pi}(1 - K_{1,2})\left[\frac{1}{r} + 2\sum_{n=1}^{\infty}\frac{K_{2,3}^{n}}{(x^2 + y^2 + 4n^2t^2)^{\frac{1}{2}}}\right] \tag{A-6}$$

$$K_{2,3} \rightarrow 1$$

Model #1, Figure A-9, indicates one of the dipole configurations used in the survey.

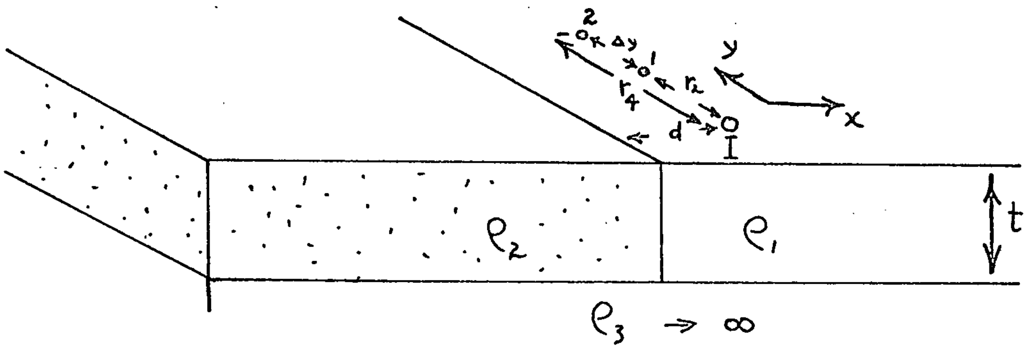

Figure A-9 Parameters for model #1

Here

$$\rho_a = \Delta U_y \frac{2\pi}{I} \left[\frac{1}{r_4} - \frac{1}{r_2} \right]^{-1} \qquad \text{(A-7)}$$

where $\Delta U_y = U(2) - U(1)$

Using the approximation

$$\Delta U_y = \frac{\partial U}{\partial y} \Delta y \qquad \text{(A-8)}$$

where Δy is the separation between measuring electrodes, and using Equation A-5 gives

$$\rho_a = r_2^{\,2} \rho_2 \left[\frac{y_2}{r_2^{\,3}} + K_{1,2} \left(\frac{y_2}{(r_2^2 + 4d^2)^{3/2}} \right) + 2 \sum_{n=1}^{\infty} y_2 K_{1,3}^{n} \left\{ \frac{1}{(r_2^{\,2} + 4n^2t^2)^{3/2}} + \frac{K_{1,2}}{(4d^2 + r_2^{\,2} + 4n^2t^2)^{3/2}} \right\} \right]$$

(A-9)

$$K_{1,3} \to 1$$

(The approximation A-8 is used to improve the convergence of the series in A-5. For infinite ρ_3, $K_{1,3}$ and $K_{2,3}$ equal unity and the potentials U_1 and U_2 become infinite. This does not mean, however, that the electric field is infinite.)

Figure A-10 shows the parameters for model #2 used in interpretation of survey results.

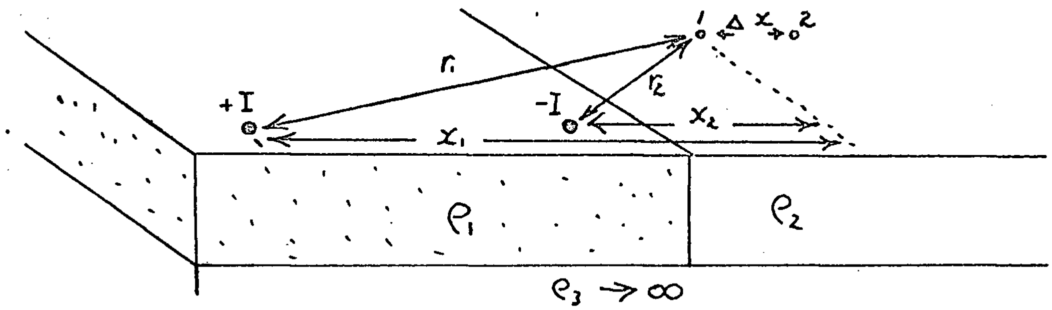

Figure A-10 Parameters for model #2.

Using Equation A-6 and

$$\Delta U_x = \frac{\partial U}{\partial x} \Delta x$$

gives

$$\rho_a = \rho_2 (1 - K_{1,2}) \left[1 + 2\left(\frac{x_2}{r_2{}^3} - \frac{x_1}{r_1{}^3}\right)^{-1} \cdot \sum_{n=1}^{\infty} K_{2,3}^{n} \left\{ \frac{x_2}{(r_2{}^2 + 4n^2t^2)^{3/2}} - \frac{x_1}{(r_1{}^2 + 4n^2t^2)^{3/2}} \right\} \right] \quad \text{(A-10)}$$

(Note that $\frac{1}{r_2} + \frac{1}{r_3} - \frac{1}{r_1} - \frac{1}{r_4} \approx \frac{x_2 \Delta x}{r_2{}^3} - \frac{x_1 \Delta x}{r_1{}^3}$)

A similar expression can be obtained for dipoles oriented in a north-south direction. Replace x_1 and x_2 by y_1 and y_2 respectively in Equation A-10.

A-3-2 Multilayer Models

Potentials for layered earth models, Figure A-11, can best be found by solving Laplace's equation ($\nabla^2 U = 0$) and then manipulating the solution into a form that can be used for numerical computations.

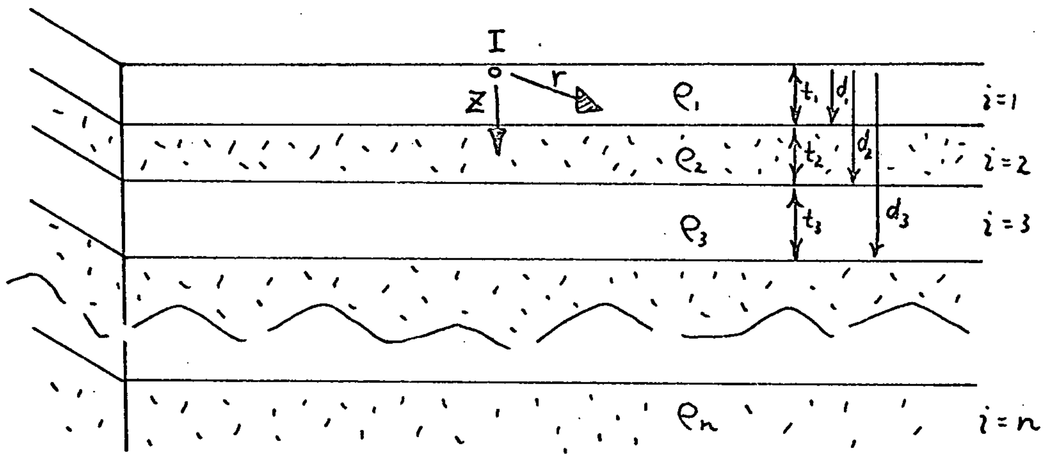

Figure A-11 Point source in an n-layer earth.

In cylindrical coordinates the solution is

$$U_i = \int_0^{\infty} [A_i(m)e^{-mz} + B_i(m)e^{mz}]J_o(mr)\,dm \qquad \text{(A-11)}$$

where m is a separation constant; J_o is a Bessel function of zero order.

In the first layer, one must add the particular solution

$$U = \frac{I\rho_1}{2\pi(r^2 + z^2)^{\frac{1}{2}}} \qquad \text{(A-12)}$$

valid near the source.

The constants A_i and B_i are determined by noting that $A_o = 0$, $B_n = 0$ and

$$U_i = U_{(i+1)} \quad \text{at } d_i$$

$$\frac{1}{\rho_i}\frac{\partial U_i}{\partial z} = \frac{1}{\rho_{(i+1)}}\frac{\partial U_{(i+1)}}{\partial z} \quad \text{at } d_i \tag{A-13}$$

The general form of the solution as found by Stefanescu [22] is

$$U(r,o) = \frac{I\rho_1}{2\pi}\left[\frac{1}{r} + 2\int_o^\infty Z(m,\ t_i,\ K_i)J_o(mr)\,dm\right] \tag{A-14}$$

$$\text{where } K_i = \frac{\rho_{i+1} - \rho_i}{\rho_{i+1} + \rho_i}$$

(An alternate form of the solution is given by E. Sunde [23].) In particular for n=3

$$Z = \frac{K_1 e^{-2mt_1} + K_2 e^{-2m(t_1+t_2)}}{1 + K_1K_2 e^{-2m(t_1+t_2)} - K_1 e^{-2mt_1} - K_2 e^{-2m(t_1+t_2)}} \tag{A-15}$$

Assuming integer values for t_1, t_2 ....t_{n-1} (this can be done without loss of generality by choosing a measuring unit which makes t_1, t_2, ...t_{n-1} integer) one expects that the kernel function, Z, can be put in the form

$$Z = \frac{P_n(e^{-2m})}{H_n(e^{-2m}) - P_n(e^{-2m})} \tag{A-16}$$

where P_n and H_n are polynomials of e^{-2m}. (This can obviously be done for the three-layer earth, A-15. The validity of this expansion is discussed by H. M. Mooney et al [18].) The polynomials are determined using the relations

$$P_{(i+1)}(e^{-2m}) = P_i(e^{-2m}) + H_i(e^{2m})K_i\ e^{-2mdi}$$

$$H_{(i+1)}(e^{-2m}) = H_i(e^{-2m}) + P_i(e^{2m})K_i\ e^{-2mdi} \qquad \text{(A-17)}$$

(H. Flathe [7])

Noting the identity

$$\int_o^\infty e^{-ma}\ J_o(mr)dm = \frac{1}{a^2 + r^2} \qquad \text{(A-18)}$$

(Laplace transform)

it is apparent that if $Z = \frac{P}{H-P}$ can be expanded in a Taylor series of the form

$$Z = \sum_{n=1}^{\infty} A_n(N)(e^{-2m})^N \qquad \text{(A-19)}$$

then the expression A-14 for the potential can be integrated term by term and the series summed to give a solution. Equating A-16 and A-19 gives

$$P_n(u) = [H_n(u) - P_n(u)] \sum_{n=1}^{\infty} A_n(N)u^N \qquad \text{(A-20)}$$

where $u = e^{-2m}$

Expanding P_n and H_n in a power series of the form

$$P_n(u) = P(1)u + P(2)u^2 \ldots P(d_{n-1})u^{d_{n-1}}$$

$$H_n(u) = 1 + H(1)u + H(2)u^2 \ldots H(d_{n-1})u^{d_{n-1}} \qquad \text{(A-21)}$$

results in the relation

$$A_n(N) = P(N) + \sum_{\ell=1}^{D} [P(\ell) - H(\ell)]A_n(N-\ell) \qquad \text{(A-22)}$$

where D is the smaller of N-1 or d_{n-1}.

The expression A-14 for the potential now becomes

$$U(r,o) = \frac{\rho_1 I}{2\pi r}\left[1 + 2\sum_{N=1}^{\infty} A_n(N)(1 + 4N^2r^{-2})^{-\frac{1}{2}}\right] \qquad \text{(A-23)}$$

From A-23 and 1-5, the apparent resistivity for a dipole array over an n-layer earth is

$$\rho_a = \rho_1\left[1 + 2\left(\frac{1}{r_1} - \frac{1}{r_2} - \frac{1}{r_3} + \frac{1}{r_4}\right)^{-1} \sum_{N=1}^{\infty} A_n(N) \cdot \right.$$

$$\left.\left\{\frac{1}{(r_1{}^2 + 4N^2)^{\frac{1}{2}}} - \frac{1}{(r_2{}^2 + 4N^2)^{\frac{1}{2}}} - \frac{1}{(r_3{}^2 + 4N^2)^{\frac{1}{2}}} + \frac{1}{(r_4{}^2 + 4N^2)^{\frac{1}{2}}}\right\}\right]$$

(A-24)

When the measuring dipoles are oriented in the x or y direction and the separation of these dipoles is small, convergence of the expression for ρ_a can be improved by using the approximations

$$\Delta U_x = \frac{\partial U}{\partial x} \Delta x$$

$$\Delta U_y = \frac{\partial U}{\partial y} \Delta y$$

A special feature of the kernel function for a three-layer earth is that for large values of resistivity in the second layer ($\rho_2 >> \rho_1, \rho_3$) the form of the function becomes dependent on $\rho_2 t_2$ not on both ρ_2 and t_2 (G. V. Keller and F. C. Frischknecht [12] p. 164, G. V. Keller [14]). The range of validity of this characteristic is given in Figure A-12 . It is therefore impossible to determine uniquely the second layer resistivity or thickness if resistivity contrasts are sufficiently large.

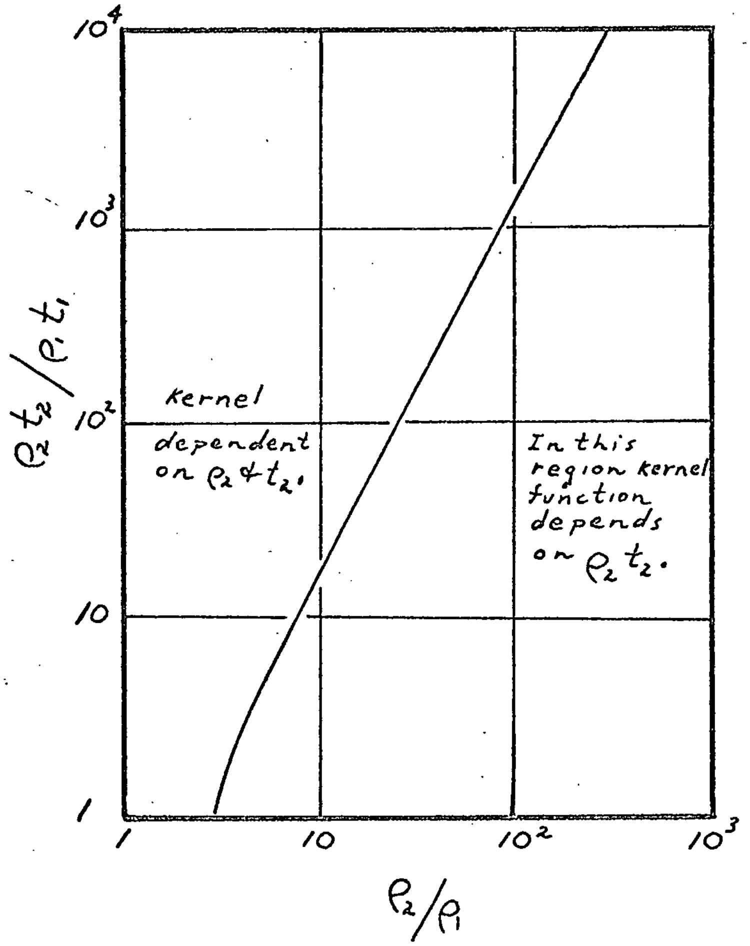

Figure A-12 Values of ρ_2 for which the three-layer kernal function depends only on $\rho_2 t_2$.

A-4 Effects of Anisotropy

In an anisotropic medium

$$j_i = - \sigma_{ik} \frac{\partial U}{\partial x_k} \qquad k=1,\ 2,\ 3 \tag{A-25}$$

where σ is conductivity.

Applying the continuity condition, one finds

$$\sigma_{ik} \frac{\partial^2 U}{\partial x_i \partial x_k} = 0 \tag{A-26}$$

Assuming the medium is transversely isotropic A-26 becomes

$$\rho_v \left[\frac{\partial^2 U}{\partial r^2} + \frac{1}{r}\frac{\partial U}{\partial r}\right] + \rho_t \frac{\partial^2 U}{\partial z^2} = 0 \tag{A-27}$$

(in cylindrical coordinates)

where ρ_v is vertical resistivity; ρ_t is transverse resistivity; z is depth.

The solution to A-25 is

$$U(r,z) = \frac{I(\rho_v\rho_t)^{\frac{1}{2}}}{2\pi(r^2 + (\rho_v/\rho_t)z^2)}$$

$$+ \int_0^\infty [A(m)e^{-(\rho_v/\rho_t)^{\frac{1}{2}}mz} + B(m)e^{(\rho_v/\rho_t)^{\frac{1}{2}}mz} J_0(mr)dm$$

(F. S. Grant and G. F. West [8]) (A-28)

This solution is identical with the solution for an isotropic medium if $(\rho_v/\rho_t)^{\frac{1}{2}}z$ is substituted for z .

Thicknesses of layers deduced from sounding curves will be in error by a factor (ρ_v/ρ_t) if resistivities are assumed to be isotropic.